information

MDPI

Article

Surveillance Radar Placement on Digital Elevation Models: A Constraint Optimization Model with a Lexicographic Coverage Objective

Youssef Kerfi [1], Mohamed Baslam [1], Kamal Bella [2] and Mouaad Mohy-eddine [3,*]

[1] Laboratory of Information Processing and Decision Support, Sultan Moulay Slimane University, Beni Mellal 23000, Morocco; kerfi.youssef@usms.ac.ma (Y.K.); m.baslam@usms.ma (M.B.)
[2] SISAR Team, LaRTiD Laboratory, Technology Higher School Essaouira, Cadi Ayyad University, Marrakech 40000, Morocco; k.bella.ced@uca.ac.ma
[3] DELTA Lab, National School of Arts and Crafts, Hassan II University, Casablanca 20670, Morocco
* Correspondence: mohy-eddine.mouaad@ensam-casa.ma

Abstract

Ground surveillance radars on rugged terrain must be placed so that a few units observe as much of the area as possible, preferably with redundancy, while remaining able to communicate. Existing models either prescribe the multiple-coverage level in advance or rely on heuristics without optimality guarantee. We formulate radar placement on a digital elevation model as a constraint optimization problem that combines line-of-sight viewsheds with antenna height and radar horizon, distance and line-of-sight constraints between radars, and a lexicographic objective that maximizes the observed area first and multiple coverage next, without a prescribed coverage level or weights. We solve it exactly with backtracking, an improved search with symmetry breaking and bounding, and a CP-SAT model, and compare them with greedy and genetic-algorithm baselines on 30 synthetic and 10 real terrains. The line-of-sight computation agrees with GDAL on 99.4% of the cells. Requiring every pair of radars to communicate directly limits the mean coverage to at most 38% on the synthetic terrains, whereas multi-hop connectivity reaches 75% with ten radars, close to the unconstrained optimum. The improved exact search solves 99 of 100 instances with up to 900 candidate locations within 300 s.

Keywords: radar placement; coverage optimization; constraint optimization problem; viewshed analysis; digital elevation model; lexicographic optimization; backtracking search; CP-SAT; multiple coverage

Check for updates

Academic Editor: Heming Jia

Received: 27 September 2026
Revised: 23 October 2026
Accepted: 2 November 2026
Published: 4 November 2026

Copyright: © 2026 by the authors. Licensee MDPI, Basel, Switzerland. This article is an open access article distributed under the terms and conditions of the Creative Commons Attribution (CC BY) license.

1. Introduction

Ground-based surveillance radars are used to monitor areas where continuous human presence is impractical or dangerous, such as borders, military sites, and remote natural environments [1,2]. The quality of the surveillance that a set of radars provides depends largely on where the radars are installed. Over irregular terrain, hills and ridges hide parts of the area from a radar even when these parts lie well within its detection range, an effect that the flat-plane disk model common in coverage studies does not capture.

Coverage measures how well a set of devices observes a region [3]. The required level of coverage depends on the application. In low-risk monitoring tasks, it may suffice that each point of the region is observed by one device (1-coverage). In security-critical

tasks, each point should be observed by several devices (k-coverage with $k > 1$), so that the failure of a single unit does not open a gap in the surveillance.

Coverage alone is not sufficient: the radars must also exchange data with one another and with a base station. Coverage and connectivity are therefore usually treated together when a deployment is planned [4,5].

When devices are dropped at random, many redundant units are needed to reach a satisfactory coverage level. When each device can be placed at a chosen location, fewer units are needed, which reduces installation and maintenance costs. Choosing these locations is, however, a combinatorial problem whose size grows quickly with the number of devices and candidate sites [6].

Most of the models that inform radar placement were developed for wireless sensor networks (WSNs). WSNs combine sensing devices such as seismic, magnetic, thermal, visual, infrared, acoustic, and radar sensors, and they support military applications (e.g., battlefield surveillance, reconnaissance, targeting, and detection of nuclear, biological, and chemical threats) as well as environmental ones (e.g., forest fire and flood detection and precision agriculture) [2]. The placement of surveillance radars on terrain raises the same coverage and connectivity questions, with the difference that terrain occlusion dominates the observable area.

Three lines of work address parts of this problem, but none of them addresses all of it. Coverage models for WSNs usually describe the sensing region as a disk on a plane and, when multiple coverage is needed, prescribe the level k in advance [3,7,8]. Observer-siting methods in geographic information systems (GIS) account for the terrain through viewsheds and maximize the jointly visible area with greedy or local-search heuristics [9,10]. Recent radar deployment studies combine detailed propagation or occlusion models with metaheuristic optimizers [11,12]. In the last two cases, the quality of a reported placement depends on the solver as much as on the model, and the distance to the optimum is unknown. We are not aware of a formulation that combines terrain-based visibility, hard distance and line-of-sight (LOS) constraints between radars, and an objective that favors multiple coverage without a prescribed k, and that is solved to proven optimality. This is the gap that the present work addresses.

In this paper, we study the placement of a fixed number of identical radars on a terrain represented by a digital elevation model (DEM). The area that a radar observes from each candidate location is computed by LOS analysis, and the placement is formulated as a constraint optimization problem (COP). Our contributions are as follows:

- **Formulation.** We formulate radar placement on a discretized DEM as a COP. The observed area of each candidate location is a viewshed computed with the antenna height, the target height, the detection range, and the radar horizon under standard atmospheric refraction. Pairwise distance and LOS constraints model the separation of the radars and their direct communication, and a multi-hop variant only requires the communication graph to be connected.
- **Objective.** We define a lexicographic objective on the coverage vector $(f_0, \ldots, f_n)$, where f_k is the number of grid points observed by exactly k radars, and prove that minimizing it is equivalent to maximizing, in lexicographic order, the number of points observed by at least one, at least two, ..., at least n radars. Neither a coverage level k nor weights need to be fixed in advance.
- **Exact solution methods.** We give an exhaustive backtracking algorithm for radar deployment (BTRD), an improved version (BTRD+) with symmetry breaking, forward checking, and an admissible bound, and a CP-SAT model solved as a sequence of lexicographic stages. The three methods return identical coverage vectors on every instance on which they complete.

https://doi.org/10.3390/info17111102

- **Reproducible evaluation.** We validate the LOS computation against the viewshed routine of GDAL and evaluate the model on 30 synthetic terrains and 10 windows of the Copernicus GLO-30 DEM. The experiments separate the effect of the constraints from that of the terrain, compare the lexicographic objective with scalar objectives and the exact methods with greedy and genetic-algorithm baselines, and include a sensitivity analysis and a scalability study. The code, data, and raw results are provided as Supplementary Materials.

The remainder of the paper is organized as follows. Section 2 reviews related work and states the research gap. Section 3 summarizes the materials and methods of the study. Section 4 recalls the definitions of constraint satisfaction and constraint optimization problems and introduces visibility analysis on DEMs. Section 5 formulates the radar placement problem and its variants. Section 6 presents the solution methods. Section 7 reports and discusses the experimental results, and Section 8 concludes the paper and outlines future work.

2. Related Work

Most of the literature on coverage-driven deployment concerns WSNs. We review it by the design dimensions that shape a coverage scheme: the type of coverage, the deployment strategy, the heterogeneity of the nodes, energy constraints, obstacles and terrain, and multiple coverage. We then discuss optimization approaches to deployment and state the research gap. In this section, we use the terms "sensor" and "node" because they are the terms of the cited literature.

2.1. Types of Coverage

Coverage schemes differ in what must be observed: an entire area, a set of discrete targets, or a barrier that intruders may cross. Area (or full) coverage requires every point of the region of interest to lie within the sensing range of at least one sensor, ideally with as few sensors as possible. Kar and Banerjee [13] achieve connected full coverage by placing sensors along strips in which neighboring sensors are separated by the sensing radius and then arranging the strips to cover the region; the regularity that this construction requires is difficult to achieve in the field.

Target coverage requires a finite set of points to be observed, a setting common in military applications. Arora et al. [14] built and tested a WSN that detects, classifies, and tracks targets. Several works study how to cover targets or areas while extending the network lifetime [15–19].

Barrier coverage concerns the detection of movements across a region. Meguerdichian et al. [20] formulated it through the maximal breach path and quantified how much additional sensors improve coverage. Chen, Kumar, and Lai [21] designed localized algorithms for barrier coverage. Sweep coverage, in which points of interest are visited periodically rather than observed continuously, is discussed in [22].

2.2. Deployment Strategies

A deployment can be dense or sparse. A dense deployment, with many nodes in the region of interest, is preferred when every event must be detected reliably or when multiple coverage is required. A sparse deployment is used when nodes are expensive or when the goal is to obtain the largest coverage from few nodes.

Nodes can be static or mobile. Howard et al. [23] proposed an incremental algorithm in which each mobile node moves to a position that increases coverage; the method requires each node to be within the sensing range of another node. In the approach of Poduri and Sukhatme [24], nodes repel their neighbors until they reach a spacing that maximizes cover-

age while preserving connectivity; its performance depends on accurate inter-node distance measurements. Osmani et al. [25] combined Voronoi diagrams and fuzzy logic to move nodes into coverage holes with limited movement, and Wang, Cao, and La Porta [4] proposed movement-assisted deployment protocols that achieve high coverage with little movement.

Finally, nodes can be placed at predetermined locations or at random, for example by dropping them from an aircraft (Figure 1). Deterministic placement makes it easier to design a coverage scheme, but it is not always possible. Bai et al. [26] derived optimal deployment patterns that achieve four-connectivity and full coverage; their analysis assumes circular sensing and communication ranges and exact node positions. Random deployments are usually dense, because extra nodes compensate for the lack of control over positions, and mobile networks often start from a random deployment and then relocate their nodes.

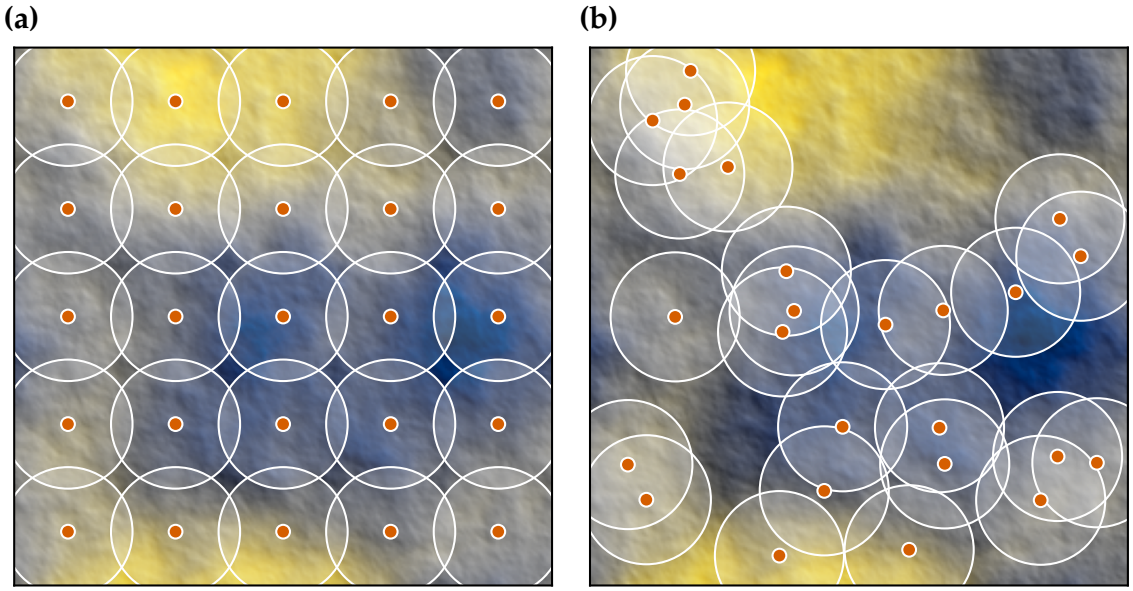


Figure 1. Deterministic and random deployments of the same number of nodes (25) over a synthetic terrain: (**a**) grid deployment; (**b**) random deployment. Color code: the background shows the elevation with hill shading, from dark blue (low) to yellow (high) (cividis color map); vermilion (red-orange) dots are the nodes, and the light disks with white outlines are their sensing ranges, all of equal radius. The random deployment leaves larger gaps and more overlap.

2.3. Node Heterogeneity

The nodes of a network can be homogeneous, with identical capabilities, or heterogeneous (Figure 2); in heterogeneous networks, a few more capable nodes, called cluster heads, often collect data from the other nodes. The constructions in [13,26] require homogeneous nodes, because the node spacing is derived from a common sensing range, and Li, Wan, and Frieder [27] study coverage algorithms for homogeneous networks. Howard et al. [23] also assume homogeneous nodes but repeat their experiments for several sensing ranges. Algorithms designed for heterogeneous networks also apply to homogeneous ones; Carbunar et al. [28], for example, detect redundant nodes and coverage boundaries with Voronoi diagrams for homogeneous sensing ranges and with weighted Voronoi diagrams for heterogeneous ones. The approach proposed in this paper assumes identical radars.

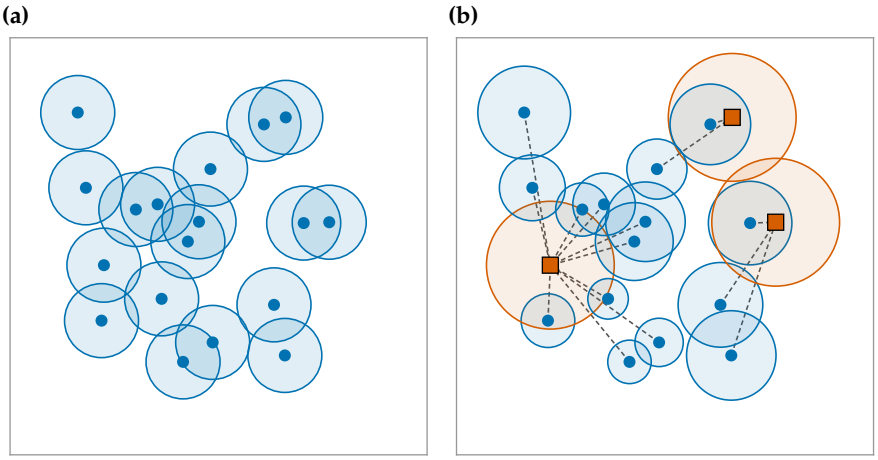


Figure 2. Homogeneous and heterogeneous networks: (**a**) homogeneous nodes with equal sensing radii; (**b**) heterogeneous nodes with different sensing radii, in which a few more capable nodes act as cluster heads (squares) that collect data from the other nodes (dashed links).

2.4. Energy Constraints

Battery-powered nodes often cannot be recharged, so many coverage schemes aim to extend the network lifetime, for example by putting redundant nodes to sleep, adjusting the sensing range, or aggregating data at cluster heads. Cardei and Wu [22] surveyed energy-efficient coverage problems. Cardei and Du [16] organize nodes into disjoint sets that are activated in turn, Xing et al. [5] proposed a protocol in which each node moves among sleep, listen, join, active, and withdraw states depending on whether it is needed for coverage, and Carbunar et al. [28] repeatedly deactivate the redundant nodes with the lowest residual energy. Our model does not include energy constraints.

2.5. Obstacles and Terrain

The sensing region of a node is usually modeled as a disk in two dimensions or a ball in three dimensions. In practice, obstacles such as walls, rocks, trees, or landforms block or reflect signals and hide the region behind them (Figure 3). Chatzigiannakis, Mylonas, and Nikoletseas [29] modeled obstacles as combinations of primitive shapes and studied their effect on routing protocols. Wang, Hu, and Tseng [30] proposed deployment algorithms that ensure coverage and connectivity with few nodes in regions with obstacles, and Zou and Chakrabarty [31] used virtual forces, including forces exerted by obstacles, to improve an initial random deployment.

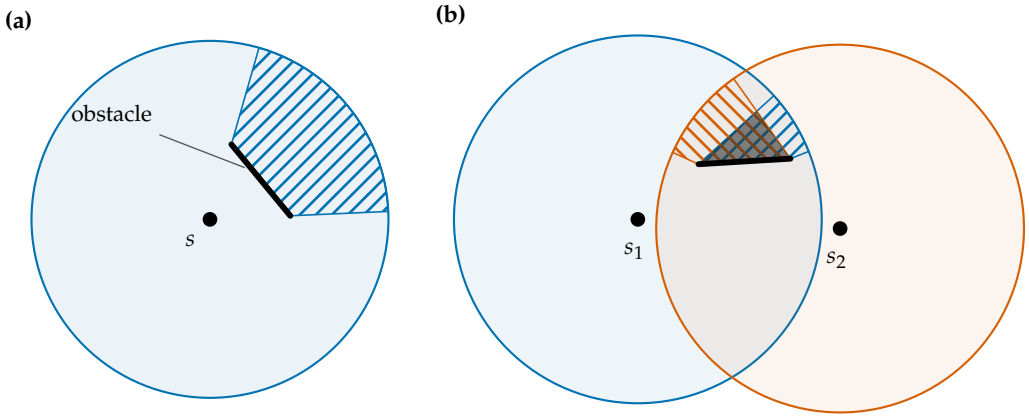


Figure 3. Effect of a line-segment obstacle on disk-shaped sensing regions: (**a**) one sensor; (**b**) two sensors sharing the same obstacle. Hatched areas are hidden from the corresponding sensor; the dark area in (**b**) is hidden from both. The shadows are computed geometrically.

On natural terrain, the relief itself is the main source of occlusion. GIS compute the viewshed of an observer, that is, the set of DEM cells visible from it; the viewshed algorithm of the GDAL library [32], for instance, follows Wang, Robinson, and White [33]. Selecting several observers whose viewsheds jointly cover as much terrain as possible is a combinatorial problem. Franklin [9] selected observers greedily among highly visible candidate points, and Kim, Rana, and Wise [10] restricted the candidates to topographic features and compared heuristics, of which simulated annealing gave the largest visible area, only slightly more than a simpler swap heuristic but at a much higher computing time. Wang and Dou [34] refined DEM-based viewsheds for wireless transmitters with a Fresnel-zone analysis and noted that base station siting combines a combinatorial optimization problem with a coverage computation. Zhou et al. [35] accelerated multi-viewshed analysis to optimize the locations of video surveillance cameras. Leenders et al. [36] reviewed probable and fuzzy viewsheds for observer location optimization and found that most approaches still rely on binary visibility.

2.6. Multiple Coverage

Some applications require every point to be observed by several sensors, a requirement known as k-coverage (Figure 4). Huang and Tseng [3] formulated the decision problem of whether every point of a region is covered by at least k sensors and gave polynomial-time algorithms that can be run as distributed protocols. Most works on k-coverage aim to preserve it while saving energy, for example by partitioning the sensors into covers that are activated in turn [37] or with randomized algorithms for dense networks [38]. Zhou, Das, and Gupta [7] considered connected k-coverage, and Nakka and Ammari [8] recently addressed connected k-coverage with heterogeneous sensors in planar networks.

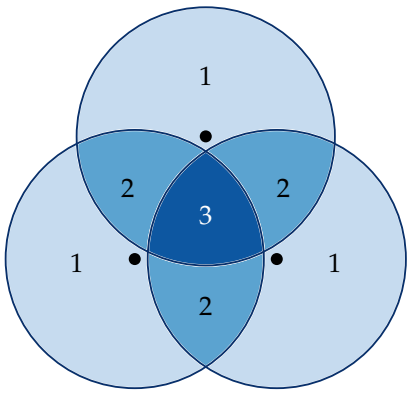


Figure 4. Multiple coverage by three sensors with equal sensing radii. Each region is labeled with its coverage multiplicity, that is, the number of sensors that observe it; the region labeled 3 is 3-covered. The regions are computed from the disk geometry.

2.7. Optimization Approaches to Deployment

In location science, the maximal covering location problem (MCLP) of Church and ReVelle [39] selects a given number of facility sites so as to maximize the demand covered within a service distance. With viewsheds as coverage sets, maximizing the number of observed points is an MCLP; our model adds pairwise constraints between the sites and replaces the single coverage count by the full coverage vector.

Deployment has been addressed with a variety of optimization techniques. Quintão, Nakamura, and Mateus [40] used an integer linear programming (ILP) formulation and an evolutionary algorithm to maintain coverage over time while managing network resources. Megerian et al. [41] combined Voronoi diagrams and graph search to compute worst- and best-case coverage in polynomial time through the maximal breach and maximal support

paths, which can guide deployment. Habib and Safar [42] split coverage into a floorplan problem, which partitions the area into candidate cells, and a placement problem, and solved the merged problem with an evolutionary approach. Dhillon and Chakrabarty [43] placed sensors on a grid so as to reach adequate coverage with a minimum number of sensors.

Recent work on radar deployment accounts more directly for propagation and terrain. Wang et al. [11] used a parabolic equation propagation model over 3D terrain and optimized a layered coverage rate with the nondominated sorting genetic algorithm III (NSGA-III). Lei, Chen, and Tan [12] defined a coverage model for frequency-modulated continuous-wave radars that includes occlusion and optimized it with the Luus–Jaakola algorithm. Abul and Savsatli [44] addressed the distribution of air-defense radars to critical areas, and Li et al. [45] combined ILP with exhaustive search to build circular barrier coverage with multistatic radars at minimum cost. For WSNs, Priyadarshi [46] proposed a particle swarm optimization (PSO) framework that balances coverage, connectivity, and energy in heterogeneous networks, and Moslehi [47] surveyed deployment strategies with respect to coverage and security. Constraint programming has also been applied to sensor placement: Löffler et al. [48] placed indoor positioning beacons with a Boolean constraint model that requires three beacons in range of every position.

2.8. Research Gap and Positioning

The works reviewed above leave three gaps for the placement of radars on terrain. First, models of multiple coverage test or impose a prescribed level k [3,7,8,48], so the trade-off between observed area and redundancy is fixed before the optimization. Second, terrain-aware siting and radar deployment methods rely on greedy, local-search, or metaheuristic optimizers [9–12], whose placements carry no optimality certificate; modeling choices and solver performance therefore cannot be assessed separately. Third, communication between devices is often described by circular ranges on a plane [26], whereas over rugged terrain two radars can communicate directly only if they see each other.

Our work addresses these gaps together: (i) the observed area is a DEM viewshed with radar-specific heights and horizon; (ii) hard distance and LOS constraints between radars model direct communication, with a multi-hop variant; (iii) a lexicographic objective on the full coverage vector favors multiple coverage without a prescribed k or weights; and (iv) exact methods, cross-checked against each other, provide optimal placements against which heuristics and alternative formulations can be measured. The price of exactness is a search whose size grows quickly with the grid and the number of radars; Section 7.8 quantifies it.

3. Materials and Methods

This study combines a problem formulation, exact and heuristic solution methods, and a computational evaluation. Section 4 recalls the background on constraint satisfaction and constraint optimization problems and on visibility analysis, Section 5 formulates the radar placement problem and its variants, and Section 6 describes the solution methods.

3.1. Materials

The evaluation uses synthetic terrains generated by spectral synthesis and real terrains extracted from the Copernicus GLO-30 DEM [49]. The line-of-sight computation is compared with the viewshed routine of GDAL [32], and the CP-SAT model is solved with Google OR-Tools [50]. All methods are implemented in Python. The terrains, the parameters, the software versions, the hardware, and the time limits are given in Section 7.1; the code, the terrain data, and the raw results are provided as Supplementary Material S1.

3.2. Use of Generative Artificial Intelligence

The generative AI tool Claude Opus 5.5 (Anthropic) was used only for language and grammar correction of the manuscript text. No generative AI tool was used in the design, implementation, or execution of the experiments, in the generation or analysis of the data, or in the production of the results, figures, or tables. The authors reviewed all corrections and take full responsibility for the content of the manuscript.

4. Preliminaries

4.1. Constraint Satisfaction and Constraint Optimization Problems

Many problems in artificial intelligence and operations research can be expressed as constraint satisfaction problems (CSPs) [51], which gives access to general solution methods. We recall the definitions used in the rest of the paper, following [52]; readers familiar with them may proceed to Section 4.2.

Definition 1 (CSP). *A constraint satisfaction problem is a triple* $\langle X, D, C\rangle$*, where* $X = \{x_1, \ldots, x_n\}$ *is a finite set of variables;* $D = \{D_1, \ldots, D_n\}$ *is a set of finite domains,* D_i *being the set of values that* x_i *can take; and* $C = \{C_1, \ldots, C_p\}$ *is a finite set of constraints on the variables of* X*.*

Definition 2 (Constraint). *A constraint* C_S *on an ordered tuple of variables* $S = (x_{s_1}, \ldots, x_{s_r})$ *is a relation on the Cartesian product of their domains,* $C_S \subseteq D_{s_1} \times \ldots \times D_{s_r}$*. The number* r *of variables in* S *is the arity of the constraint.*

Constraints of arity two (binary constraints) can be represented by a constraint graph whose vertices are the variables and whose edges are the constraints, and any CSP can be transformed into an equivalent CSP with only unary and binary constraints [53].

Definition 3 (Instantiation and solution). *An instantiation of* X *is an* n*-tuple* $\Gamma = (a_1, \ldots, a_n)$ *with* $a_i \in D_i$ *for all* i*; we write* $\Gamma(x_i) = a_i$*. The instantiation* Γ *satisfies a constraint* C_S *on* $S = (x_{s_1}, \ldots, x_{s_r})$ *if* $(\Gamma(x_{s_1}), \ldots, \Gamma(x_{s_r})) \in C_S$*, and it is a solution of the CSP if it satisfies every constraint of* C*.*

Example 1 (Map coloring). *The regions of a map must be colored so that adjacent regions receive different colors. For the four regions of Figure 5a and three colors,* $X = \{x_1, x_2, x_3, x_4\}$ *and* $D_1 = D_2 = D_3 = D_4 = \{\text{red}, \text{green}, \text{blue}\}$*. The constraint that* x_1 *and* x_2 *receive different colors is*

$$C_{x_1,x_2} = \{(u, v) \in D_1 \times D_2 \mid u \neq v\}, \tag{1}$$

and C_{x_1,x_3}*,* C_{x_1,x_4}*,* C_{x_2,x_4}*, and* C_{x_3,x_4} *are defined in the same way; regions* x_2 *and* x_3 *are not adjacent and are not constrained. The instantiation* $\Gamma = (\text{red}, \text{green}, \text{green}, \text{blue})$ *satisfies all five constraints and is a solution (Figure 5b shows the constraint graph).*

A CSP may be over-constrained, in which case no solution exists, or it may admit many solutions of which some are preferable to others. Constraint optimization problems handle both situations by attaching valuations to the combinations of values.

Definition 4 (COP). *A constraint optimization problem is a quadruple* $\langle X, D, C, R\rangle$*, where* X *and* D *are defined as in a CSP;* $C = \{C_1, \ldots, C_p\}$ *is a finite set of hard constraints; and* $R = \{R_1, \ldots, R_s\}$ *is a finite set of soft constraints, each soft constraint* R_i *on the variables* $(x_{i_1}, \ldots, x_{i_l})$ *being a function*

$$R_i \colon D_{i_1} \times \ldots \times D_{i_l} \to \mathbb{R} \tag{2}$$

that assigns a weight to each combination of values. A solution of a COP is an instantiation that satisfies all hard constraints and optimizes (maximizes or minimizes) the objective function, usually defined as the sum of the weights of the soft constraints.

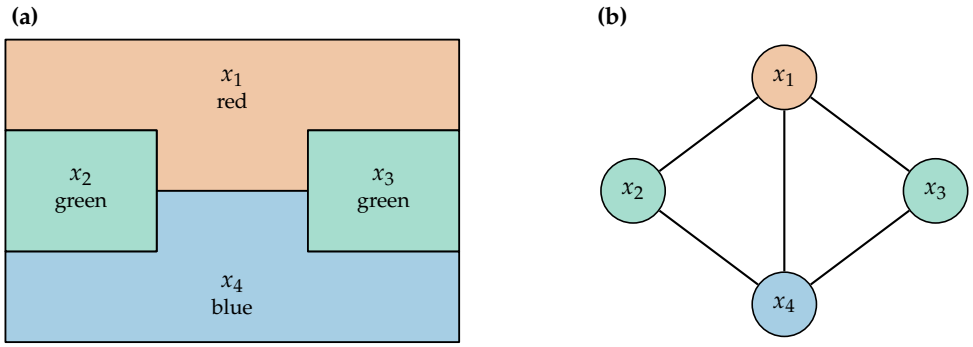


Figure 5. Map-coloring example: (**a**) a map with four regions, colored with the solution $\Gamma = (\text{red}, \text{green}, \text{green}, \text{blue})$; (**b**) the corresponding constraint graph, with one edge per pair of adjacent regions.

In Section 5, we replace the scalar sum by a vector-valued objective compared in lexicographic order, a standard way of ranking objectives by strict priority [54].

4.2. Visibility Analysis on Digital Elevation Models

A DEM represents a terrain as a 2.5D surface: an elevation is given at the center of each cell of a regular planar grid with spacing Δ, and elevations between cell centers are obtained by bilinear interpolation. We write $z(s)$ for the elevation at a planimetric position s. Visibility on a DEM is based on the line of sight: two points are intervisible if the straight segment that joins them does not pass below the terrain surface. We write $\text{los}(p, q) = \text{true}$ when points p and q are intervisible and $\text{los}(p, q) = \text{false}$ otherwise.

Figure 6 illustrates these notions on a terrain profile. Point p_3 is visible from p_1, because the segment p_1p_3 lies above the surface ($\text{los}(p_1, p_3) = \text{true}$). Point p_2 is not visible from p_1, because an intermediate hill intersects the segment p_1p_2 ($\text{los}(p_1, p_2) = \text{false}$). Likewise, p_4 is hidden from p_1 by the ridge that culminates at p_3 ($\text{los}(p_1, p_4) = \text{false}$), although p_4 is at a higher elevation than p_2.

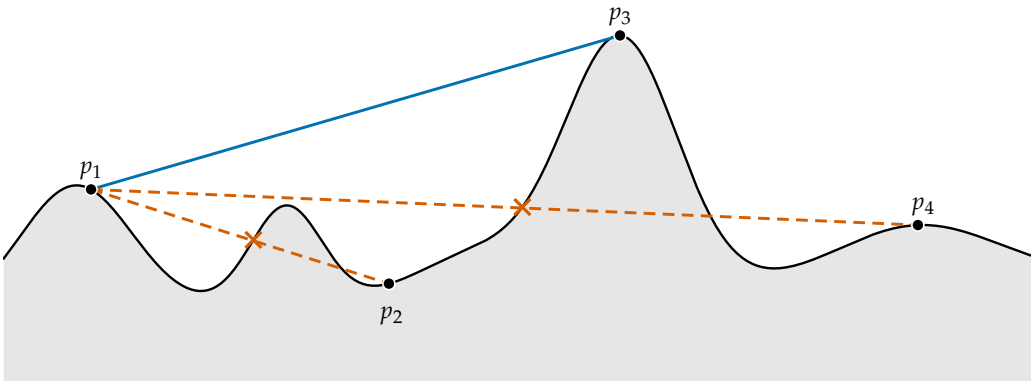


Figure 6. Line of sight on a terrain profile. Solid lines are unobstructed sight lines and dashed lines are obstructed ones; crosses mark where an obstructed line first meets the terrain. Point p_3 is visible from p_1, whereas p_2 and p_4 are not.

4.2.1. Line-of-Sight Test

Let an observer at planimetric position p have its antenna at height h_p above the ground, let a target at q be at height h_q above the ground, and let $D = d(p, q)$ be the planimetric (horizontal) distance between them. As is standard for radar propagation, Earth curvature and atmospheric refraction are accounted for by an effective Earth radius

κR_E, with $R_E = 6371$ km and $\kappa = 4/3$ for a standard atmosphere [55,56]. The target is visible from the observer, $\mathrm{los}(p, q) = \text{true}$, if

$$z(s) + \frac{s\,(D-s)}{2\kappa R_E} \;\le\; z(p) + h_p + \frac{s}{D}\big(z(q) + h_q - z(p) - h_p\big) \tag{3}$$

at every point of the segment at distance $s \in (0, D)$ from p. The left-hand side is the terrain raised by the Earth bulge, and the right-hand side is the sight line. The condition is symmetric in p and q, and we check it at points spaced at most $\Delta/2$ apart. Over smooth terrain and for a ground target ($h_q = 0$), it reduces to $D \le \sqrt{2\kappa R_E h_p}$, the radar horizon of an antenna at height h_p. Radar coverage uses the antenna height $h_p = h_r$ and the target height $h_q = h_t$, and communication between two radars uses $h_p = h_q = h_r$.

4.2.2. Viewsheds

We discretize the region of interest into a set I of points arranged in an $m \times m$ grid and numbered row by row from 1 to m^2 (Figure 7); each grid point is placed at the center of the DEM cell that contains it. For a radar with detection radius R, the visibility indicator of a pair of points $(p, q) \in I^2$ is

$$v(p, q) = \begin{cases} 1 & \text{if } \mathrm{los}(p, q) = \text{true and } d(p, q) \le R, \\ 0 & \text{otherwise,} \end{cases} \tag{4}$$

where los is evaluated with heights h_r at p and h_t at q, and $d(p, q)$ is the planimetric Euclidean distance. The detection radius R is the maximum range at which the radar detects the reference target, which follows from the radar range equation for that target and the radar parameters [55]. The viewshed of a radar placed at point p is the set of grid points that it observes:

$$V_p = \{q \in I \mid v(p, q) = 1\}. \tag{5}$$

Figure 8 illustrates Equations (4) and (5) for a single location of one of the experimental terrains: the viewshed is fragmented by the relief and much smaller than the disk of radius R.

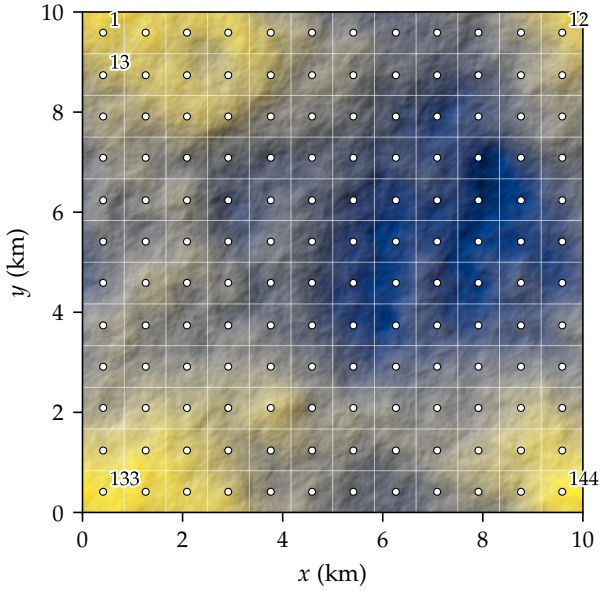


Figure 7. Discretization of the region of interest. The terrain (synthetic terrain 1 of the experiments, 10×10 km; elevation from dark blue, low, to yellow, high, with hill shading) is overlaid with an $m \times m$ grid ($m = 12$); each grid point is a candidate radar location, numbered row by row from 1 to m^2

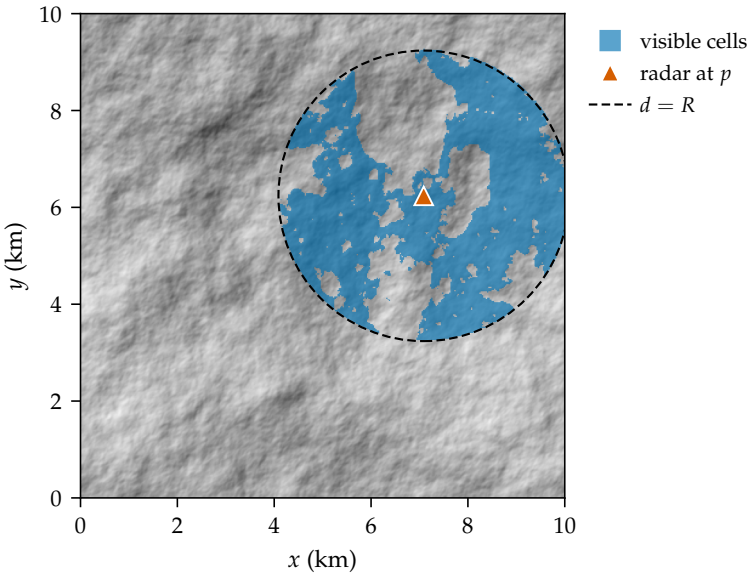


Figure 8. Viewshed of a single radar on synthetic terrain 1, computed at the resolution of the DEM with the parameters of Section 7.1. The radar (triangle) observes the highlighted cells, which satisfy both the LOS condition (3) and $d(p, q) \leq R$; the dashed circle has radius $R = 3$ km. Gray levels show the hill-shaded relief.

Remark 1 (Radar-specific elements)**.** *Like the disk models of WSN coverage and the viewsheds of observer siting, the detection model* (4) *is binary and geometric. Five of its ingredients are specific to radar: (i) a target is detected only if the direct path from the antenna is not masked by the terrain, which is modeled by the LOS test* (3)*; (ii) the antenna height h_r and the target height h_t set the coverage of low-altitude targets; (iii) the effective Earth radius models the radar horizon under standard refraction; (iv) R is the detection range of the reference target; and (v) the minimum distance between radars (Section 5.1) limits mutual interference. Clutter, multipath, diffraction, and the probability of detection as a function of the signal-to-noise ratio are not modeled. Because the formulation and the solution methods use only the binary values $v(p, q)$, a finer detection model, for example a detection probability above a threshold computed with a propagation model [11], can replace Equation* (4) *without other changes.*

5. Problem Formulation

We consider the placement of n identical radars on a terrain represented by a DEM and discretized as in Section 4.2. In security applications, points observed by several radars remain monitored if one radar fails, so the model should favor such points once the observed area has been maximized. Table 1 summarizes the notation.

Table 1. Notation.

Symbol	Meaning
I, m	Set of grid points (candidate locations and points to observe), $\lvert I\rvert = m^2$
n	Number of radars
x_i, $D(x_i)$	Location of radar $i \in \{1, \ldots, n\}$ (decision variable) and its domain $\{1, \ldots, m^2\}$
A	Assignment of locations to (some of) the variables $x_1, \ldots, x_n$
$d(p, q)$, $\mathrm{los}(p, q)$	Planimetric distance and line-of-sight predicate between points p and q, Equation (3)
h_r, h_t	Radar antenna height and target height above the ground
R	Detection radius of a radar
$d_{\min}$, $d_{\max}$	Minimum and maximum distance between two radars

Table 1. *Cont.*

Symbol	Meaning
$v(p,q)$, V_p	Visibility indicator and viewshed, Equations (4) and (5)
$c_A(q)$	Coverage multiplicity of point q under A, Equation (8)
$f_k(A)$, $N_k(A)$	Number of points observed by exactly k and by at least k radars, Equations (9) and (13)
$<_{\text{lex}}$	Strict lexicographic order, Equation (11)

5.1. Variables, Domains, and Hard Constraints

Each radar i is associated with a variable x_i whose value is the index of the grid point where the radar is installed. An assignment A gives values to some of the variables; it is complete when all n variables have a value. The following hard constraints must hold for every pair of distinct radars:

$$d_{\min} \le d(x_i, x_j) \le d_{\max} \qquad \forall i, j \in \{1, \dots, n\},\ i \neq j, \tag{6}$$

$$\text{los}(x_i, x_j) = \text{true} \qquad \forall i, j \in \{1, \dots, n\},\ i \neq j. \tag{7}$$

The lower bound in Equation (6) keeps radars apart to limit interference and overlapping transmissions, and, since $d_{\min} > 0$, it prevents two radars from sharing a location. The upper bound and Equation (7) ensure that every pair of radars can communicate directly.

Remark 2. *Imposing the upper bound of Equation (6) and the LOS constraint (7) on every pair of radars makes the communication graph complete (full mesh). This condition is sufficient for network connectivity but conservative: a connected communication graph, in which radars may relay each other's data, would suffice. The pairwise upper bound also confines all radars to a region of diameter at most $d_{\max}$. Section 5.3 defines the multi-hop variant.*

5.2. Coverage Multiplicity and Lexicographic Objective

For a complete assignment A, the coverage multiplicity of a point $q \in I$ is the number of radars that observe it:

$$c_A(q) = \left|\{i \in \{1, \dots, n\} \mid q \in V_{x_i}\}\right|. \tag{8}$$

A point q is k-covered by A if $c_A(q) \ge k$, and A achieves k-coverage of I if every point of I is k-covered. For $k \in \{0, 1, \dots, n\}$, let

$$f_k(A) = \left|\{q \in I \mid c_A(q) = k\}\right| \tag{9}$$

be the number of points observed by exactly k radars. Every point has exactly one multiplicity, hence

$$\sum_{k=0}^{n} f_k(A) = m^2. \tag{10}$$

The coverage vector of A is $f(A) = (f_0(A), f_1(A), \dots, f_n(A))$. In COP terms, each variable x_i carries a soft constraint whose valuation is the viewshed V_{x_i}, and the valuations are combined into the coverage vector instead of a scalar sum.

Coverage vectors are compared in lexicographic order. For $a, b \in \mathbb{N}^{n+1}$,

$$a <_{\text{lex}} b \iff \exists k \in \{0, \dots, n\} : a_k < b_k \text{ and } a_l = b_l\ \forall l < k, \tag{11}$$

and $a \le_{\text{lex}} b$ if $a <_{\text{lex}} b$ or $a = b$; $a >_{\text{lex}} b$ means $b <_{\text{lex}} a$. Let $\mathcal{F}$ be the set of complete assignments that satisfy Equations (6) and (7). The radar placement problem is

$$\operatorname*{lex\,min}_{A\in\mathcal{F}} \; f(A) = \big(f_0(A), f_1(A), \ldots, f_n(A)\big), \tag{12}$$

that is, find $A^* \in \mathcal{F}$ such that $f(A^*) \leq_{\text{lex}} f(A)$ for all $A \in \mathcal{F}$. The lexicographic order first minimizes the number f_0 of unobserved points; among placements with the same f_0, it minimizes the number f_1 of points observed by a single radar, and so on.

The effect of this order on multiple coverage is made precise by the number of points observed by at least k radars,

$$N_k(A) = \big|\{q \in I \mid c_A(q) \geq k\}\big| = \sum_{l=k}^{n} f_l(A), \qquad k \in \{1, \ldots, n\}. \tag{13}$$

The coverage rate reported in Section 7 is $100\, N_1(A)/m^2 = 100\,(1 - f_0(A)/m^2)$ percent.

Proposition 1. *For any $A, B \in \mathcal{F}$, $f(A) <_{\text{lex}} f(B)$ if and only if $(N_1(A), \ldots, N_n(A)) >_{\text{lex}} (N_1(B), \ldots, N_n(B))$.*

Proof. By Equations (10) and (13), every complete assignment A satisfies

$$N_{k+1}(A) = m^2 - \textstyle\sum_{l=0}^{k} f_l(A), \qquad k \in \{0, \ldots, n-1\}, \tag{14}$$

$$f_k(A) = N_k(A) - N_{k+1}(A), \qquad k \in \{0, \ldots, n\}, \tag{15}$$

with the conventions $N_0(A) = m^2$ and $N_{n+1}(A) = 0$.

($\Rightarrow$) Assume $f(A) <_{\text{lex}} f(B)$ and let k be the first index at which the two vectors differ, so that $f_k(A) < f_k(B)$ and $f_l(A) = f_l(B)$ for all $l < k$. If k were equal to n, Equation (10) would give $f_n(A) = m^2 - \sum_{l<n} f_l(A) = f_n(B)$, a contradiction; hence $k \leq n-1$. By Equation (14), $N_l(A) = N_l(B)$ for all $l \in \{1, \ldots, k\}$, because these values depend only on $f_0, \ldots, f_{l-1}$, and $N_{k+1}(A) = N_{k+1}(B) + f_k(B) - f_k(A) > N_{k+1}(B)$. Therefore $(N_1(A), \ldots, N_n(A)) >_{\text{lex}} (N_1(B), \ldots, N_n(B))$, with first difference at index $k+1$.

($\Leftarrow$) Assume $(N_1(A), \ldots, N_n(A)) >_{\text{lex}} (N_1(B), \ldots, N_n(B))$ and let j be the first index at which they differ, so that $N_j(A) > N_j(B)$ and $N_l(A) = N_l(B)$ for all $l < j$. By Equation (15), $f_l(A) = f_l(B)$ for all $l < j-1$, and $f_{j-1}(A) = N_{j-1}(A) - N_j(A) < N_{j-1}(B) - N_j(B) = f_{j-1}(B)$. Therefore $f(A) <_{\text{lex}} f(B)$, with first difference at index $j-1$. □

Proposition 1 shows that the objective (12) maximizes the number of points observed by at least one radar, then, among the placements that achieve this maximum, the number of points observed by at least two radars, and so on. Once f_0 is fixed, the total $\sum_{k\geq 1} f_k = m^2 - f_0$ is fixed as well, and reducing f_1 moves observed points toward higher multiplicities; this does not imply that every component $f_2, \ldots, f_n$ increases individually. The objective favors multiple coverage without requiring a prescribed level k; k-coverage of I is not imposed as a constraint. Example 2 illustrates these definitions.

Example 2. *Table 2 gives the vectors f and N of three hypothetical placements A, B, and C of $n = 3$ radars on a grid of $m^2 = 16$ points. Placements A and B leave the same number of points unobserved ($f_0 = 4$), and $f(A) <_{\text{lex}} f(B)$ because $f_1(A) = 6 < 8 = f_1(B)$; equivalently, $N_1(A) = N_1(B) = 12$ and $N_2(A) = 6 > 4 = N_2(B)$: among the 12 observed points, A observes more of them at least twice. Placement C observes more points at least twice than A ($N_2(C) = 8$), but it leaves one more point unobserved ($f_0(C) = 5$) and is therefore ranked last: the lexicographic order never trades observed area for redundancy. The ranking is A, B, C.*

Table 2. Coverage vectors f and vectors N of the three hypothetical placements of Example 2 ($n = 3$, $m^2 = 16$), and their rank in the lexicographic order.

	f_0	f_1	f_2	f_3	N_1	N_2	N_3	**Rank**
A	4	6	4	2	12	6	2	1
B	4	8	2	2	12	4	2	2
C	5	3	4	4	11	8	4	3

5.3. Multi-Hop Variant and Reference Relaxations

Two radars can communicate directly if they are within distance $d_{\max}$ of each other and intervisible. For a complete assignment A, let G_A be the graph on the n radars whose edges join the pairs $\{i, j\}$ with $d(x_i, x_j) \leq d_{\max}$ and $\mathrm{los}(x_i, x_j) = \text{true}$. The constraints (6) and (7) require G_A to be complete; we refer to them as the full-mesh (FM) model. The multi-hop (MH) variant keeps the lower bound for every pair and only requires G_A to be connected, so that radars may relay each other's data:

$$d(x_i, x_j) \geq d_{\min} \qquad \forall i, j \in \{1, \ldots, n\},\ i \neq j, \tag{16}$$

$$G_A \text{ is connected.} \tag{17}$$

Every FM-feasible placement is MH-feasible. To separate the effect of the constraints from that of the terrain, we also use two relaxations as references: DM, which keeps only the minimum distance (16), and UC, which only requires distinct locations; and a flat terrain, on which, for the parameters of Section 7.1, only the detection radius limits the viewsheds. The objective (12) is the same in all cases. For every variant and every n, $N_1(A) \leq \bar{N} = |\bigcup_{p \in I} V_p|$, the number of points observable from at least one candidate location.

6. Solution Methods

We solve problem (12) and its variants exactly with three methods: the exhaustive backtracking search BTRD (Sections 6.1 and 6.2), the improved search BTRD+ (Section 6.3), and a CP-SAT model solved in lexicographic stages (Section 6.4). Greedy and genetic-algorithm baselines are described in Section 6.5.

6.1. Exhaustive Backtracking (BTRD)

BTRD, given in Algorithm 1, is a depth-first search based on chronological backtracking. It extends a partial assignment one variable at a time. Each new value must be consistent with the values already assigned, that is, the extended assignment must satisfy every hard constraint (6) and (7) between the new radar and the radars already placed. When no value of the current variable is consistent, the search reaches a dead end and returns to the previous variable, which receives its next value. The search is exhaustive: it does not stop at the first complete consistent assignment, but evaluates all of them and keeps the best one. We keep BTRD as a transparent reference implementation of the model, whose behavior follows directly from the definitions.

The search starts with an incumbent vector $f^* = (+\infty, \ldots, +\infty)$, which every coverage vector precedes lexicographically; any vector worse than all feasible ones, such as $(m^2 + 1, 0, \ldots, 0)$, can be used instead. Whenever a complete assignment is reached, its coverage vector is computed and compared with the incumbent; if it precedes the incumbent in the order (11), it becomes the new incumbent. In our implementation, the number of observed points N_1 of a complete assignment is computed first, and the full vector only when N_1 is not smaller than that of the incumbent, which gives the same comparison outcome. An inconsistent value is simply skipped, and the variable x_i is released when the recursive call returns, so no explicit unassignment step is needed.

Algorithm 1 BTRD: exhaustive backtracking search for a lexicographically optimal placement.

Input: grid I; viewsheds V_p for all $p \in I$; number of radars n; $d_{\min}$, $d_{\max}$
Output: placement A^* and its coverage vector f^*

$A^* \leftarrow \emptyset$; $f^* \leftarrow (+\infty, \ldots, +\infty)$ ▷ *worse than every coverage vector*
$L \leftarrow$ the points of I sorted by decreasing viewshed size $|V_p|$ ▷ *value ordering*
SEARCH($\emptyset$, 1)
return A^*, f^*

function SEARCH(A, i) ▷ *A assigns $x_1, \ldots, x_{i-1}$*
  if $i = n + 1$ **then** ▷ *A is complete*
    $f \leftarrow$ COVERAGEVECTOR(A)
    if $f <_{\text{lex}} f^*$ **then**
      $A^* \leftarrow A$; $f^* \leftarrow f$ ▷ *new incumbent*
    end if
    return
  end if
  for all $v \in L$ **do** ▷ *candidate locations for x_i*
    if CONSISTENT(A, v) **then**
      SEARCH($A \cup \{x_i \leftarrow v\}$, $i + 1$) ▷ *x_i is unassigned on return*
    end if
  end for
end function

function CONSISTENT(A, v)
  return true if $d_{\min} \le d(u, v) \le d_{\max}$ and $\text{los}(u, v)$ for every value u assigned in A, else **false**
end function

function COVERAGEVECTOR(A)
  $c(q) \leftarrow |\{i \mid q \in V_{x_i}\}|$ for all $q \in I$ ▷ *Equation (8)*
  return $(f_0, \ldots, f_n)$ with $f_k = |\{q \in I \mid c(q) = k\}|$ ▷ *Equation (9)*
end function

The value-ordering heuristic is static: it tries the locations with the largest viewsheds first. It does not change the result of a complete search, but it tends to produce good incumbents early, which matters if the search is interrupted.

6.2. Correctness and Complexity

BTRD enumerates every complete assignment that satisfies the hard constraints and keeps the lexicographically smallest coverage vector, so it returns an optimal solution of (12) when it runs to completion. Apart from the hard-constraint checks, the search uses no bounding or propagation. In the worst case, it therefore visits $O((m^2)^n)$ complete assignments. With the viewsheds and the pairwise distances and LOS values precomputed, a consistency check costs $O(n)$ and a coverage vector costs $O(n\,m^2)$, for a worst-case running time of $O((m^2)^n\, n\, m^2)$. For $m = 12$ and $n = 10$, $(m^2)^n \approx 3.8 \times 10^{21}$. Because the radars are identical, each placement is also generated up to $n!$ times, once per permutation of the radars; imposing $x_1 < x_2 < \ldots < x_n$ removes this symmetry, but the number of placements is still $\binom{m^2}{n} \approx 7.7 \times 10^{14}$ for the same values. The hard constraints prune part of this space; Section 7.8 measures how much.

6.3. Improved Exact Search (BTRD+)

BTRD checks the hard constraints only against the radars already placed and evaluates every complete assignment. BTRD+ (Algorithm 2) adds three standard techniques that preserve exactness.

Symmetry breaking. The radars are identical, so $f(A)$ depends only on the set of locations. BTRD+ assigns locations in increasing order of their position in L, which enumerates each set once instead of $n!$ times [57].

Forward checking. For the next radar, BTRD+ keeps the list of locations that follow the last assigned one in L and are compatible with every radar already placed [58]. A branch whose list has fewer elements than the number of radars still to be placed is pruned.

Bounding. Let C be the set of points observed by the radars already placed and k the number of radars still to place. Any completion observes at most $|C|$ plus the sum of the k largest marginal gains $|V_p \setminus C|$ over the candidate list. If this bound is smaller than N_1 of the incumbent, no completion can precede the incumbent in the lexicographic order (Proposition 1), and the branch is pruned. The incumbent is initialized with the placement found by the multi-start greedy heuristic of Section 6.5, when that heuristic finds a feasible placement.

Algorithm 2 BTRD+: exhaustive search with symmetry breaking, forward checking, and bounding.

Input: as in Algorithm 1; optional initial placement $A_0 \in \mathcal{F}$
Output: placement A^* and its coverage vector f^*

$A^* \leftarrow A_0$ and $f^* \leftarrow f(A_0)$ if A_0 is given, else $A^* \leftarrow \emptyset$ and $f^* \leftarrow (+\infty, \ldots, +\infty)$
$L \leftarrow$ the points of I sorted by decreasing $|V_p|$
SEARCH+($\emptyset$, L, $\emptyset$, n)
return A^*, f^*

function SEARCH+(A, Λ, C, k) ▷ Λ: *candidates;* $C = \bigcup_{x \in A} V_x$; k *radars left*
  if $k = 0$ **then**
    if $f(A) <_{\text{lex}} f^*$ **then** $A^* \leftarrow A$; $f^* \leftarrow f(A)$ **end if**; **return**
  end if
  if $|\Lambda| < k$ **then return** ▷ *forward checking*
  end if
  if $|C| +$ (sum of the k largest $|V_p \setminus C|$, $p \in \Lambda$) $< N_1(A^*)$ **then return** ▷ *bound*
  end if
  for $j = 1, \ldots, |\Lambda| - k + 1$ **do**
    $v \leftarrow \Lambda_j$; $\Lambda' \leftarrow (\Lambda_{j'} \mid j' > j,\ \Lambda_{j'}$ compatible with $v)$ ▷ *order of L kept*
    SEARCH+($A \cup \{v\}$, Λ', $C \cup V_v$, $k - 1$)
  end for
end function

6.4. CP-SAT Model Solved in Lexicographic Stages

Since the problem is stated as a COP, general-purpose solvers can also be applied once the model is written in their input language, for example MiniZinc [59]. We use the CP-SAT solver of Google OR-Tools [50,60] with the following 0–1 model. A Boolean variable y_p indicates a radar at $p \in I$, and $z_{q,k}$ ($q \in I$, $k = 1, \ldots, n$) indicates that q is observed by at least k radars:

$$\sum_{p \in I} y_p = n, \tag{18}$$

$$y_p + y_{p'} \le 1 \qquad \forall \{p, p'\} \subseteq I \text{ that violate (6) or (7)}, \tag{19}$$

$$\sum_{p \in I} v(p,q)\, y_p \ge k\, z_{q,k} \qquad \forall q \in I,\ k \in \{1, \ldots, n\}, \tag{20}$$

$$z_{q,k} \le z_{q,k-1} \qquad \forall q \in I,\ k \in \{2, \ldots, n\}. \tag{21}$$

In any solution, $N_k \ge \sum_q z_{q,k}$, with equality when $\sum_q z_{q,k}$ is maximized. The lexicographic objective is solved in stages: stage k maximizes $\sum_q z_{q,k}$ subject to (18)–(21) and $\sum_q z_{q,l} \ge N_l^*$ for all $l < k$, where N_l^* is the optimal value of stage l, and the stages stop when $N_k^* = 0$. By Proposition 1, the final solution is optimal for (12); this is the usual sequential solution of a lexicographic problem [54]. A single weighted objective $\sum_k w_k \sum_q z_{q,k}$ with $w_k = (m^2+1)^{n-k}$ would be equivalent, but for $m = 12$ and $n = 10$ its largest weight, $145^9 \approx 2.8 \times 10^{19}$, exceeds the range of the 64-bit integers used by the solver.

For the MH variant, constraint (19) is restricted to pairs closer than $d_{\min}$, and connectivity (17) is enforced by vertex-separator inequalities added on demand. Let G be the communication graph on I, with an edge between every pair of locations within $d_{\max}$ of each other and intervisible. If the radars of a solution S induce a disconnected subgraph of G, let K be one of its connected components, $u \in K$, and $w \in S \setminus K$, and let Γ be the set of locations outside K that are adjacent to K and connected to w in G without K. Every connected placement that contains u and w contains a location of Γ, so

$$y_u + y_w - 1 \leq \sum_{s \in \Gamma} y_s \tag{22}$$

is valid for the MH variant and violated by S. A stage is solved again after these inequalities are added, until its optimal solution is connected; that solution is then optimal for the MH variant, since the inequalities only remove disconnected placements.

6.5. Heuristic Baselines

Greedy. Starting from a location p, the greedy heuristic repeatedly adds the location, compatible with all radars already placed, that gives the lexicographically largest $(N_1, \ldots, N_n)$; it fails if no compatible location remains before n radars are placed. We run it from every $p \in I$ and keep the best placement (multi-start greedy), and we also report the single run that starts from the location with the largest viewshed (Greedy-1). Without pairwise constraints, the greedy maximization of N_1 has a $(1 - 1/e)$ approximation guarantee, because the number of observed points is a submodular function of the set of locations [61]; the pairwise constraints remove this guarantee.

Genetic algorithm (GA). Individuals are sets of n distinct locations, ranked lexicographically by (number of violated pairs, $f_0, \ldots, f_n$), so that feasibility comes first and coverage next. The initial population of 60 individuals is built by randomized feasible construction: random locations are added if they are compatible with those already chosen, and a random location is added when none is. Each generation keeps the 2 best individuals and creates the others by tournament selection (size 3) and crossover, which applies the same construction to the union of the two parents' locations; with probability 0.3, a mutation then moves one radar to a random free location, chosen with probability 1/2 within two grid steps of its current location and otherwise anywhere on the grid. The GA runs for 200 generations and is repeated with 10 random seeds.

7. Experimental Results and Discussion

7.1. Experimental Setup

7.1.1. Terrains

All terrains cover a square domain of 10×10 km represented by 400×400 DEM cells of $\Delta = 25$ m. The 30 synthetic terrains are fractional Brownian surfaces generated by spectral synthesis with spectral exponent $\beta = 4.2$ and random seeds 1 to 30, scaled to a relief (maximum minus minimum elevation) of 600 m (Figure 9a). The 10 real terrains come from the Copernicus GLO-30 DEM [49]: the $1^\circ \times 1^\circ$ tile N32 W007, around Beni Mellal (Morocco), was reprojected to UTM zone 29N at 25 m with bilinear resampling and cut into 80 non-overlapping 10×10 km windows without missing data, and the windows at the relief deciles 5%, 15%, …, 95% were selected, so that the real terrains range from a plain (relief 50 m) to mountains (relief 1419 m) (Figure 9b). A flat terrain is used as a reference without occlusion.

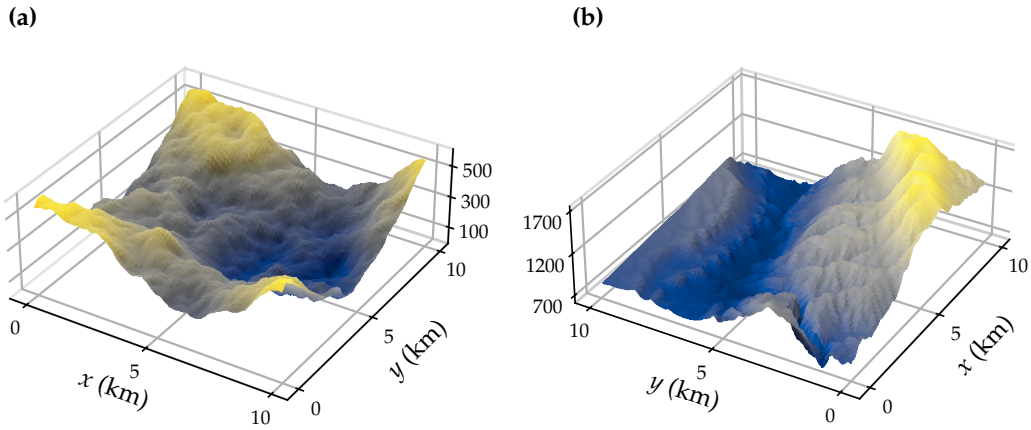


Figure 9. Examples of experimental terrains (10 × 10 km; vertical axis: elevation in meters; color from dark blue, low, to yellow, high): (**a**) synthetic terrain 1; (**b**) real terrain 9, extracted from the Copernicus GLO-30 DEM (relief 1127 m).

7.1.2. Parameters

Table 3 lists the parameters. They do not describe a specific radar: they were fixed before the experiments so that a single detection disk covers about 28% of the domain, and Section 7.7 varies each of them. The detection radius R, the distances $d_{\min}$ and $d_{\max}$, and the heights h_r and h_t are the same for all instances, except in the sensitivity analysis. With $m = 12$, neighboring grid points are 833 m apart, so $d_{\min} = 1$ km forbids radars at horizontally or vertically adjacent grid points.

Table 3. Parameters of the experiments (Section 7.7 varies R, $d_{\min}$, $d_{\max}$, h_r, h_t, κ, the relief, and β; Section 7.8 varies m).

Parameter	Symbol	Value
Domain side; DEM cell size	L; Δ	10 km; 25 m (400 × 400 cells)
Grid points per side; number of radars	m; n	12; 2 to 10
Detection radius	R	3 km
Minimum and maximum distance between radars	$d_{\min}$; $d_{\max}$	1 km; 5 km
Antenna height; target height	h_r; h_t	10 m; 2 m
Effective Earth radius factor	κ	4/3
LOS sampling step		$\Delta/2 = 12.5$ m
Terrains		30 synthetic, 10 real, 1 flat

7.1.3. Implementation

All methods are implemented in Python 3.12 with NumPy. CP-SAT is the solver of Google OR-Tools 9.15 [50], run with eight threads unless stated otherwise; BTRD, BTRD+, the greedy heuristics, and the GA are single-threaded. The validation uses GDAL 3.12.2 [32]. All runs were made on an Apple M4 Pro processor (12 cores) with 24 GB of memory. Each run has a time limit of 600 s in Sections 7.3, 7.6, and 7.7, and of 300 s in Sections 7.5 and 7.8. Every placement reported below was checked again against all hard constraints, and every MH placement against connectivity. The code, the real terrain windows, and the results of every run are provided as Supplementary Materials.

7.2. Validation of the Line-of-Sight Computation

Our LOS test (3) is implemented directly from its definition. To check it against an established GIS tool, we compared it with the viewshed routine of GDAL [32] (`GDALViewshedGenerate`, used by the `gdal_viewshed` utility), with the same DEM, observer and target heights, detection radius, and curvature correction (GDAL curvature coefficient $1/\kappa = 0.75$, or 0 for a flat Earth). On three synthetic and three real terrains, we computed the viewsheds of 20 random observers per terrain at the full resolution of the DEM and compared every cell within distance $R - \Delta$ of the observer, 5,336,280 cells in total; we also compared the visibility matrix $v(p, q)$ of the model on the 12×12 grid, for all 4212 ordered pairs of distinct grid points within distance R per terrain. Table 4 gives the results and Figure 10 shows one observer.

Table 4. Agreement between our LOS computation and GDAL. Cell level: share of DEM cells within distance $R - \Delta$ of 20 observers on which the two viewsheds agree, with curvature ($\kappa = 4/3$) and without it (flat Earth), and share of the disagreements located on a visibility boundary of our viewshed (cells with a neighbor of different visibility). Grid level: agreement of the matrix $v(p, q)$ of the model. Step: agreement between our test with sampling steps $\Delta/2$ and $\Delta/10$.

		Cell Level			Grid Level	Step
Terrain	**Relief (m)**	**Agree, $\kappa = 4/3$ (%)**	**Agree, Flat (%)**	**On Boundary (%)**	**Agree (%)**	**Agree (%)**
Synthetic 1	600	99.23	99.23	92.9	99.41	99.81
Synthetic 2	600	99.38	99.38	95.0	99.45	99.91
Synthetic 3	600	99.40	99.39	95.1	99.45	99.88
Real 3	114	98.86	98.86	95.4	99.26	99.93
Real 7	490	99.87	99.88	97.9	99.93	100.00
Real 10	1419	99.53	99.53	94.9	99.72	99.95

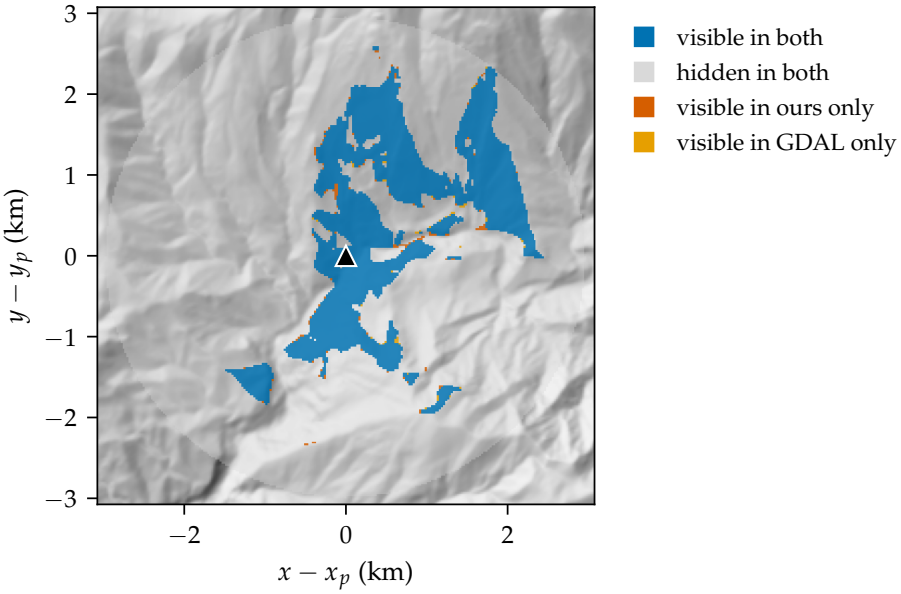


Figure 10. Comparison of our viewshed with GDAL's for one observer (triangle) at the center of real terrain 10 ($R = 3$ km, $h_r = 10$ m, $h_t = 2$ m, $\kappa = 4/3$). The two viewsheds agree on 99.53% of the 44,469 cells compared; the disagreements are mostly on the edges of visible regions. Gray levels show the hill-shaded relief.

The two computations agree on 98.86% to 99.87% of the cells (99.38% overall), and 94.8% of the disagreements lie on a visibility boundary, where the two methods discretize the terrain differently: GDAL computes visibility outward from the observer with reference

planes defined by the cells already processed, without tracing individual sight lines [33], whereas we test each sight line on the bilinearly interpolated surface. On the grid of the model, the matrices $v(p, q)$ agree on 99.26% to 99.93% of the pairs. Reducing the sampling step from $\Delta/2$ to $\Delta/10$ changes at most 0.19% of the pairs. With the parameters of Table 3, the curvature correction has almost no effect (on synthetic terrains 1–10, the mean viewshed is 8.66 grid points without it and 8.65 with it), because the Earth bulge does not exceed $R^2/(8\kappa R_E) \approx 0.13$ m at the middle of a 3 km sight line; since the bulge grows with the square of the distance, the correction matters for longer ranges. Our implementation is slower than GDAL (about 0.27 s vs. 5 ms per full-resolution viewshed), but viewsheds are computed once per instance, before the search.

7.3. Coverage vs. the Number of Radars

Figure 11 and Table 5 report the coverage rate $100\,N_1/m^2$ of the lexicographically optimal placements computed by CP-SAT, for 2 to 10 radars, on the 30 synthetic and the 10 real terrains. All 1476 runs of this section were solved to optimality or proven infeasible within the time limit, except 22; for these, the time limit was reached in a later stage of the lexicographic optimization, and N_1 and N_2 of the reported placements are optimal.

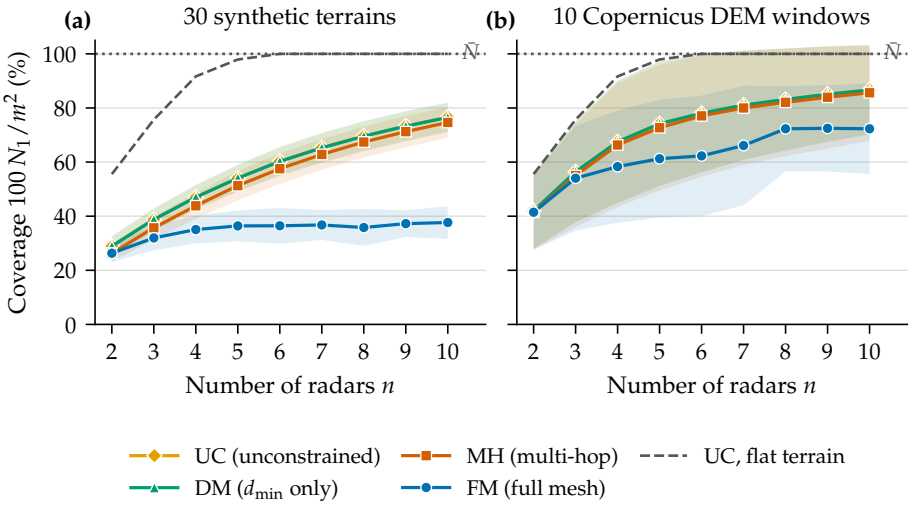


Figure 11. Coverage rate of the lexicographically optimal placements vs. the number of radars: mean over the terrains (lines) and ± one standard deviation (bands), for the full-mesh model (FM), the multi-hop variant (MH), the minimum-distance-only variant (DM), and the unconstrained variant (UC); FM means are taken over the terrains on which FM is feasible (Table 5). The dashed line is UC on a flat terrain, and the dotted line $\bar{N}$ is the mean visibility ceiling. (**a**) 30 synthetic terrains; (**b**) 10 real terrains.

Replication. With the full-mesh model of the original formulation, coverage on the synthetic terrains rises from 26.3% with two radars to 35.1% with four and then stays almost constant, between 35.8% and 37.7% on average for 5 to 10 radars. The plateau is not an artifact of one terrain: the number of radars that maximizes the FM coverage lies between 4 and 8 on every synthetic terrain, and adding a radar *reduces* the optimal coverage in 55 of the 267 cases in which both placements are feasible (synthetic and real terrains). This is possible because every radar must be within $d_{\max}$ of, and see, every other radar: a larger set must be more compact, and the best set of $n + 1$ mutually visible locations need not contain the best set of n. Beyond some n, no such set exists: FM is infeasible for 22 of the 30 synthetic terrains with 10 radars.

Table 5. Coverage rate (%) of the lexicographically optimal placements: mean (standard deviation) over the terrains. A superscript gives the number of terrains on which the model is feasible when it is smaller than the total; "infeasible" means that no terrain admits a feasible placement. $\bar{N}$: visibility ceiling $100\,\bar{N}/m^2$.

Terrains	Model	$n = 2$	$n = 4$	$n = 6$	$n = 8$	$n = 10$
Synthetic (30)	FM	26.3 (3.2)	35.1 (5.1)	36.5 (6.6)	35.8 (6.8)^{24}	37.7 (6.1)^{8}
	MH	26.3 (3.2)	43.8 (4.8)	57.5 (5.6)	67.4 (5.7)	74.7 (5.7)
	DM	28.9 (3.6)	47.0 (4.5)	60.3 (5.3)	69.6 (5.6)	76.5 (5.5)
	UC	28.9 (3.6)	47.0 (4.5)	60.3 (5.2)	69.6 (5.4)	76.6 (5.2)
	$\bar{N}$	100.0 on every terrain				
Real (10)	FM	41.5 (13.9)	58.3 (20.8)	62.3 (22.3)	72.3 (15.8)^{8}	72.3 (16.8)^{8}
	MH	41.5 (13.9)	66.3 (22.9)	77.1 (22.5)	82.1 (19.9)	85.6 (17.8)
	DM	42.0 (14.1)	67.5 (22.6)	78.1 (21.9)	83.1 (18.8)	86.6 (16.4)
	UC	42.0 (14.1)	67.5 (22.6)	78.1 (21.9)	83.1 (18.8)	86.7 (16.4)
	$\bar{N}$	100.0 on every terrain				
Flat	FM	54.9	79.2	85.4	88.2	88.2
Flat	UC	55.6	91.7	100.0	100.0	100.0

7.4. Effect of the Constraints and of the Terrain

The variants of Section 5.3 separate the two explanations of the plateau that the first version of this study could not distinguish. If terrain occlusion limited the coverage, relaxing the constraints would not help, and the visibility ceiling $\bar{N}$ would be close to the coverage achieved. The opposite is observed. On every terrain, synthetic or real, every grid point is visible from at least one candidate location ($\bar{N} = m^2$). With multi-hop connectivity (MH), coverage keeps increasing with n and reaches 74.7% (synthetic) and 85.6% (real) with ten radars, against 76.6% and 86.7% without any constraint (UC). Requiring only a connected communication graph thus recovers almost all the coverage lost to the full mesh: the mean gap between UC and MH is at most 3.2 percentage points for every n, whereas MH exceeds FM by 21.1 points with six radars on the synthetic terrains. The minimum distance alone (DM) costs almost nothing compared with UC. The plateau of the full-mesh model is therefore caused by the pairwise $d_{\max}$ and LOS constraints, not by the terrain: when additional radars do not improve coverage, the full-mesh communication requirement is the first modeling choice to question.

The terrain still matters, but through the size of the viewsheds rather than through a hard limit. On the flat terrain, where only the detection radius limits the viewsheds, six unconstrained radars observe the whole grid, and four already observe 91.7%; on the synthetic terrains, the same four radars observe 47.0% on average. Even without terrain, the full-mesh model stops at 88.2%, because the upper bound $d_{\max}$ confines all radars to a region of diameter 5 km. Real terrains, which include plains and valleys, lie in between (67.5% with four radars).

Figure 12 shows the optimal FM and MH placements of six radars on real terrain 8, and Table 6 gives their coverage vectors f and the corresponding vectors N, together with the UC optimum. Each vector sums to $m^2 = 144$ (Equation (10)). The FM radars form a compact cluster whose members all see each other; the MH radars spread along chains of intervisible locations and observe 20 more points.

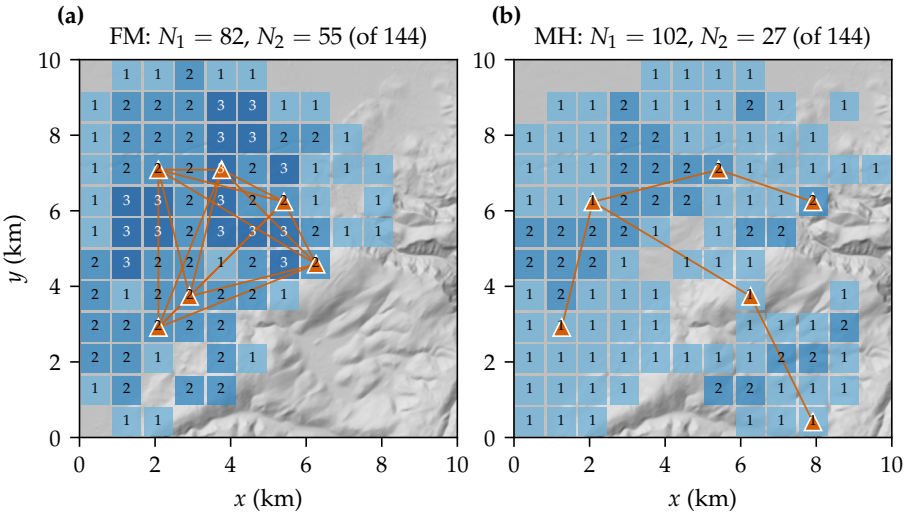


Figure 12. Optimal placements of six radars (triangles) on real terrain 8: (**a**) full-mesh model; (**b**) multi-hop variant. Lines join radars that can communicate directly ($d \leq d_{\max}$ and LOS). Squares mark the grid points observed by at least one radar; the number is the coverage multiplicity $c_A(q)$, and darker blue means a higher multiplicity. Gray levels show the hill-shaded relief.

Table 6. Coverage vectors f and vectors N of the lexicographically optimal placements of $n = 6$ radars on real terrain 8 for the full-mesh model (FM), the multi-hop variant (MH), and the unconstrained variant (UC).

	f_0	f_1	f_2	f_3	f_4	f_5	f_6	N_1	N_2	N_3	N_4	N_5	N_6
FM	62	27	39	16	0	0	0	82	55	16	0	0	0
MH	42	75	27	0	0	0	0	102	27	0	0	0	0
UC	33	95	12	4	0	0	0	111	16	4	0	0	0

7.5. Comparison of the Solution Methods

Table 7 compares the solution methods on 15 terrains (synthetic terrains 1–10 and real terrains 2, 4, 6, 8, and 10) with the FM model. The reference optimum is the CP-SAT result with eight threads.

Table 7. Comparison of the solution methods (FM model, 15 terrains, time limit 300 s per run). Feas.: terrains on which FM is feasible. Exact methods: number of runs solved to optimality or proven infeasible (Done) and median time over the 15 runs in seconds, including runs stopped at the limit. Greedy (multi-start; one run per feasible terrain) and GA (10 seeds per feasible terrain): number of runs whose coverage vector is lexicographically optimal/whose N_1 is optimal, and mean coverage gap to the optimum in percentage points (pp) over the runs that found a feasible placement.

		BTRD		BTRD+		CP-SAT, 8 thr.		CP-SAT, 1 thr.		Greedy		GA	
n	Feas.	Done	Time	Done	Time	Done	Time	Done	Time	Opt.	Gap	Opt.	Gap
2	15	15	0.00	15	0.00	15	0.1	15	0.6	15/15	0.00	122/122	0.39
3	15	15	0.04	15	0.00	15	0.3	15	1.1	15/15	0.00	109/119	0.50
4	15	15	0.4	15	0.00	15	0.4	15	0.8	14/14	0.05	91/95	0.70
5	15	15	2.9	15	0.00	15	0.3	15	0.5	13/13	0.14	97/110	0.53
6	15	12	12	15	0.00	15	0.3	15	0.5	11/12	0.28	85/95	0.61
7	15	10	34	15	0.01	15	0.4	15	0.6	11/11	0.88	92/103	0.64
8	10	9	68	15	0.01	15	0.4	15	0.6	7/7	0.23	50/51	0.88
9	7	9	84	15	0.01	15	0.3	15	0.5	3/4	0.89	38/42	0.80
10	6	8	159	15	0.00	15	0.3	15	0.5	3/3	0.42	27/30	0.84

Exact methods. The three exact methods return the same coverage vector whenever they complete: all 378 completed runs of BTRD and BTRD+ (with and without the greedy warm start) match the CP-SAT optimum. Their running times differ by orders of magnitude. BTRD, which checks the constraints only against the radars already placed and generates every placement $n!$ times, completes all runs up to $n = 5$ but only 8 of the 15 runs with $n = 10$ within 300 s; the median number of nodes it explores grows from 961,685 for $n = 5$ to 7,273,043 for $n = 10$. When it is stopped, its incumbent is already lexicographically optimal in 17 of the 26 truncated runs on feasible instances (and has the optimal N_1 in 19), which suggests that the value ordering finds good placements early; but the search cannot certify them. BTRD+ completes every run, in at most 8.17 s: symmetry breaking, forward checking, and the bound reduce the median number of nodes for $n = 5$ from 961,685 to 1196, and the greedy warm start has little effect (BTRD+ without it also completes every run). CP-SAT with eight threads solves every instance in at most 2.3 s (median 0.25 s). With a single thread, CP-SAT also solves every instance of this comparison, in at most 7.1 s (median 0.45 s). Its performance on the other variants depends more on parallelism: in a preliminary run, CP-SAT with four threads did not prove the second lexicographic stage of an unconstrained instance (synthetic terrain 1, $R = 2$ km, $n = 4$) within 600 s, whereas eight threads solve it in less than a second; all other experiments therefore use eight threads.

Heuristics. The heuristics are fast but not exact. Multi-start greedy, which runs the greedy construction from every grid point, finds the lexicographic optimum in 92 of the 113 runs on feasible instances; it fails to find any feasible placement in 2 of them, all with $n \geq 8$, because the full-mesh constraints leave few completions to a greedy partial placement. A single greedy run from the location with the largest viewshed (Greedy-1) is much worse: it is lexicographically optimal in 27 of 113 runs and fails in 36. The GA finds a feasible placement in 1130 of 1130 runs and stays close to the optimum (mean gap 0.62 percentage points), but it reaches the lexicographic optimum in 711 of these runs only, in at most 3.4 s per run. On the 12×12 grids, the exact methods are thus as fast as the heuristics and always optimal; Section 7.8 examines larger grids.

7.6. Lexicographic vs. Scalar Objectives

To assess what the lexicographic objective brings, we solved three scalar alternatives with CP-SAT on the same instances (FM model, 40 terrains, $n \in \{4, 6, 8, 10\}$): MCLP, which maximizes N_1 only; SUM, which maximizes the total multiplicity $\sum_q c_A(q) = \sum_k N_k$, that is, the sum of the viewshed sizes of the radars (a weighted-sum objective with equal weights); and K2, which maximizes the number N_2 of 2-covered points, as a model with a prescribed level $k = 2$ would. For SUM and K2, ties are broken in favor of the largest N_1, which gives these objectives their best case; for MCLP, we computed the smallest and the largest N_2 over all placements that maximize N_1. Table 8 summarizes the results.

Table 8. Lexicographic vs. scalar objectives (FM model; means over the terrains on which FM is feasible). For MCLP, N_1 equals the lexicographic optimum; the table gives the smallest N_2 over the MCLP-optimal placements and the number of terrains on which this smallest N_2 is below the lexicographic one. For SUM and K2, the placement with the largest N_1 among the optimal ones. All values are numbers of grid points (out of $m^2 = 144$).

		Lexicographic		**MCLP**		**SUM**		**K2**	
n	**Terrains**	N_1	N_2	**min** N_2	**# Below**	N_1	N_2	N_1	N_2
4	40	58.9	18.1	15.8	19	49.0	26.4	45.6	30.8
6	40	61.8	32.2	29.4	25	53.1	32.5	54.9	39.4
8	32	64.7	43.4	40.8	14	57.6	38.6	60.6	46.8
10	16	79.2	58.1	56.3	7	74.1	51.9	75.4	61.5

Table 8 shows what each part of the lexicographic objective contributes. MCLP reaches the same observed area as the lexicographic objective, since its N_1 is optimal by construction, but it does not control redundancy: on 19 of the 40 terrains with four radars and 25 of 40 with six, some placements that maximize N_1 observe fewer points at least twice than the lexicographic optimum, and a solver that maximizes N_1 only may return any of them. SUM, which rewards every observation equally, gives up observed area on almost every terrain (on 40 of 40 with four radars, by 9.9 points on average); with eight or more radars, it even observes fewer points at least twice than the lexicographic optimum (38.6 vs. 43.4 for $n = 8$). K2 behaves as a model with a prescribed level $k = 2$: with four radars, it observes 12.6 more points twice than the lexicographic optimum but 13.2 fewer points at all. The lexicographic objective is thus the only one of the four that keeps the largest observed area and, among the placements that achieve it, the largest redundancy, without any parameter. Its cost is computational, since it requires up to n solves instead of one: in the CP-SAT runs of Section 7.3 on these instances, the lexicographic solve took 0.61 s on average (at most 5.8 s), against 0.07 s for its first stage, which is the MCLP problem.

7.7. Sensitivity Analysis

Figure 13 varies one parameter at a time around the values of Table 3, on synthetic terrains 1–10, for four and eight radars, with the FM model and, for the parameters that act on the viewsheds, the unconstrained variant UC.

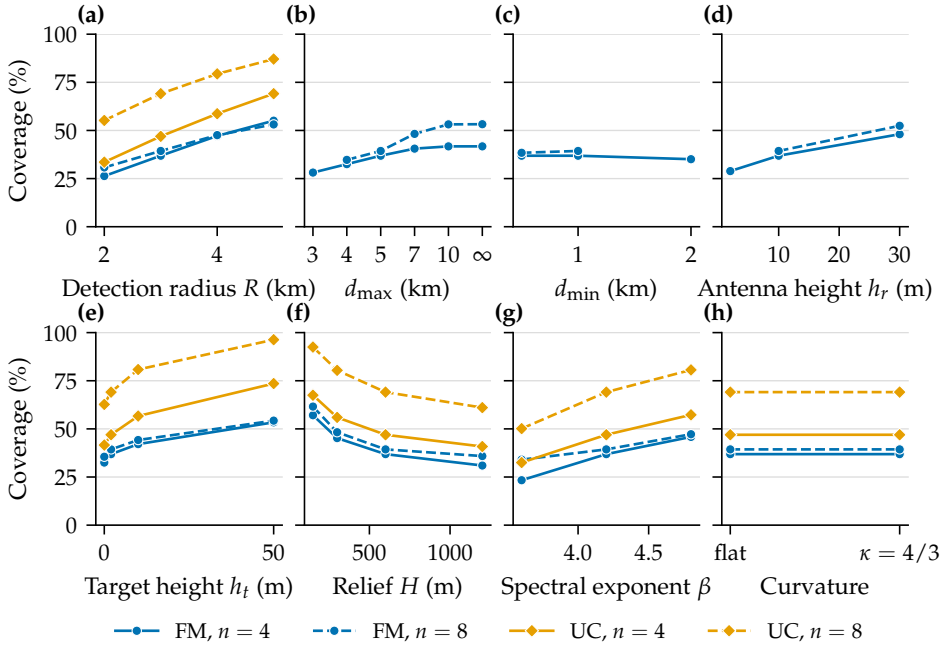


Figure 13. Sensitivity of the optimal coverage rate to one parameter at a time (mean over synthetic terrains 1–10; FM means over the terrains on which FM is feasible): (**a**) detection radius; (**b**) maximum distance between radars; (**c**) minimum distance; (**d**) antenna height; (**e**) target height; (**f**) terrain relief; (**g**) spectral exponent of the terrain (larger is smoother); (**h**) flat Earth vs. effective Earth radius $\kappa = 4/3$. A missing point means that FM is infeasible on all ten terrains.

The optimal coverage depends strongly on the parameters that shape the viewsheds. Increasing the detection radius from 2 to 5 km raises the coverage of eight unconstrained radars from 55.2% to 87.1% and that of four FM radars from 26.3% to 55.1%. The target height has a comparable effect: low targets are hidden by small relief features, so the mean viewshed grows from 7.2 grid points for ground targets ($h_t = 0$) to 18.3 for targets 50 m above the ground, and the coverage of eight unconstrained radars from 62.7% to 96.3%. Raising the antenna from 2 to 30 m increases the coverage of four FM radars from 28.9% to

48.1%. Higher or rougher terrain reduces coverage: from a relief of 150 m to 1200 m, the coverage of eight unconstrained radars drops from 92.5% to 61.0%, and from the smoothest ($\beta = 4.8$) to the roughest ($\beta = 3.6$) terrains, from 80.6% to 50.1%.

The distance constraints act on the full-mesh model mainly through feasibility. With eight radars, FM is infeasible on all ten terrains when $d_{\max} = 3$ km, $d_{\min} = 2$ km, or $h_r = 2$ m (missing points in Figure 13b–d), whereas $d_{\max} = 7$ km makes it feasible on nine of the ten terrains and raises its coverage to 48.2%; removing the upper bound ($d_{\max} = \infty$) gives 53.2%, still well below the 69.1% of the unconstrained placements, because the LOS constraint between every pair of radars remains. Finally, the Earth-curvature correction does not change the optimal coverage at the ranges considered here, since the bulge of the Earth does not exceed 0.13 m on a 3 km sight line; it matters for longer detection ranges.

7.8. Scalability and Pruning

To measure how the methods scale, we kept the 10×10 km domain and refined the grid from $m = 12$ to $m = 30$ (from 144 to 900 candidate locations), on synthetic terrains 1–5 with 4 to 10 radars. Table 9 reports the results; the effect of the hard constraints on the size of the search space is measured first.

Table 9. Scalability on synthetic terrains 1–5 (FM model, time limit 300 s per run). CP-SAT (eight threads) and BTRD+: runs solved to optimality or proven infeasible out of 5, and median time in seconds. Greedy (multi-start) and GA (3 seeds): mean gap in N_1 to the best CP-SAT placement, in percentage points of m^2.

		CP-SAT		BTRD+		Greedy	GA
m	n	Done	Time (s)	Done	Time (s)	Gap (pp)	Gap (pp)
12	4	5/5	0.2	5/5	0.00	0.00	0.74
12	6	5/5	0.3	5/5	0.00	0.00	0.74
12	8	5/5	0.4	5/5	0.01	0.00	0.93
12	10	5/5	0.06	5/5	0.00	–	–
16	4	5/5	1.1	5/5	0.01	0.00	1.33
16	6	5/5	1.0	5/5	0.02	0.00	0.96
16	8	5/5	1.5	5/5	0.04	0.55	0.99
16	10	5/5	2.9	5/5	0.04	0.00	0.24
20	4	5/5	7.7	5/5	0.02	0.00	0.60
20	6	5/5	6.4	5/5	0.1	0.05	0.62
20	8	5/5	8.0	5/5	0.3	0.20	1.12
20	10	5/5	14	5/5	0.6	0.15	0.57
25	4	5/5	114	5/5	0.06	0.00	1.02
25	6	5/5	59	5/5	0.5	0.00	1.05
25	8	5/5	65	5/5	2.0	0.00	1.61
25	10	5/5	80	5/5	4.0	1.73	1.49
30	4	5/5	141	5/5	0.1	0.00	2.07
30	6	4/5	165	5/5	1.3	0.40	0.89
30	8	5/5	115	5/5	11	0.36	1.59
30	10	4/5	113	4/5	32	0.47	1.87

Pruning by the hard constraints. The pairwise constraints remove most of the search space. On the 12×12 grid, the full-mesh constraints are satisfied by 11.9% of the pairs of locations on average, and only 1405 to 8596 of the 17,178,876 sets of four locations are feasible on terrains 1–5, a fraction of at most 5.0×10^{-4}. On the 30×30 grid, 12.3% of the pairs are compatible, and between 4,215,443 and 20,282,583 of the 2.72×10^{10} sets of four locations are feasible (fraction at most 7.5×10^{-4}). The proportion of compatible pairs stays at about 12% for every m, so the number of feasible placements grows with the number of

candidate locations roughly as fast as the number of all placements, which is what makes larger instances hard.

Running times. CP-SAT solves 98 of the 100 runs to optimality or proves them infeasible within 300 s; with four radars, its median time grows from 0.2 s for $m = 12$ to 141 s for $m = 30$. BTRD+ completes 99 of 100 runs and is much faster on the larger grids: with four radars and $m = 30$, its median time is 0.1 s, and with ten radars 32 s, one run reaching the limit. The bound on N_1 of BTRD+ is thus very effective for the FM model; CP-SAT, in exchange, also handles the MH variant, whose connectivity constraint BTRD+ does not support. The heuristics remain fast (less than 1 s on average for both greedy and the GA at $m = 30$) and close to the optimum in observed area (mean gaps of at most 1.7 and 2.1 percentage points, Table 9), but they give no certificate. The viewsheds and radar-to-radar LOS values are computed once per instance, in 2.5 s for the 900 locations of the 30×30 grid. These results indicate that exact solution is practical for areas of the size studied here (10×10 km with a few hundred candidate locations and up to ten radars). For larger regions, finer grids, or larger networks, the exact methods will need stronger bounds, such as bounds on the whole coverage vector rather than on N_1 only, or a decomposition of the region; the heuristics can then be used, and their quality measured on smaller instances solved exactly.

7.9. Limitations

The study has several limitations. First, the detection model is binary and geometric: clutter, multipath, diffraction, and the probability of detection are not modeled (Remark 1), and errors in the DEM make visibility uncertain in practice [36]. Second, the terrain is static, the radars are identical, and energy is not considered. Third, candidate locations and observed points share one grid, so coverage is measured at m^2 points rather than over the continuous surface, and the results depend on the grid resolution. Fourth, the real terrains come from a single region (one tile of the Copernicus DEM) and the synthetic ones from one family of fractal surfaces; other landscapes, such as urban areas with buildings, may behave differently. Fifth, the parameters are illustrative rather than those of a specific radar, although the sensitivity analysis shows how the results change with each of them. Finally, the exact methods were evaluated up to 900 candidate locations and 10 radars; larger regions, finer grids, or larger networks will require stronger bounds, decomposition of the region, or heuristics without optimality guarantee, whose results can then be compared with exact solutions of smaller instances.

8. Conclusions and Future Work

We have formulated the placement of surveillance radars on a terrain represented by a DEM as a constraint optimization problem that combines radar viewsheds (with antenna and target heights and the radar horizon), distance and LOS constraints between radars, and a lexicographic objective on the coverage vector. We have shown that this objective maximizes, in lexicographic order, the number of points observed by at least one, two, . . . , n radars, so that neither a coverage level k nor weights need to be fixed in advance, and we have solved the model and a multi-hop variant exactly with an exhaustive backtracking search, an improved search with symmetry breaking, forward checking, and bounding, and a CP-SAT model solved in lexicographic stages.

The experiments, on 30 synthetic terrains and 10 windows of the Copernicus GLO-30 DEM, support four conclusions. First, the LOS computation agrees with the viewshed routine of GDAL on 99.4% of the cells, the disagreements lying on visibility boundaries. Second, the coverage plateau of the full-mesh model is caused by the requirement that every pair of radars communicate directly, not by the terrain: with multi-hop connectivity,

coverage keeps increasing with the number of radars and stays within 3.2 percentage points of the unconstrained optimum on average. Third, the lexicographic objective keeps the largest observed area, which a weighted sum of multiplicities and a fixed-k objective do not, and selects among the corresponding placements one with the largest redundancy, which maximizing the observed area alone does not guarantee; its price is a sequence of solves instead of one. Fourth, exact solution is practical at the scale studied: on grids of up to 900 candidate locations with up to 10 radars, the improved search and CP-SAT solve 99 and 98 of the 100 instances within 300 s, and they show that the heuristic baselines, although close in observed area, are not reliable for the full objective: the genetic algorithm misses the lexicographic optimum in 37% of its runs on the 12×12 grids.

Future work will address the limitations of Section 7.9: probabilistic detection and DEM uncertainty, heterogeneous radars, prescribed k-coverage as a hard constraint, and larger regions, for which stronger bounds on the whole coverage vector, decomposition of the region, and the use of exact solutions of small instances to calibrate heuristics are natural directions.

Supplementary Materials: The following supporting information can be downloaded at: https://www.mdpi.com/article/10.3390/info17111102/s1, Supplementary Material S1: source code of the model, the solution methods, and the experiments; the derived terrain windows; and the raw results of all runs.

Author Contributions: Conceptualization, Y.K. and M.B.; methodology, Y.K.; software, Y.K.; validation, Y.K., K.B. and M.M.-e.; formal analysis, Y.K. and K.B.; investigation, Y.K.; data curation, Y.K. and M.M.-e.; writing—original draft preparation, Y.K.; writing—review and editing, M.B., K.B. and M.M.-e.; visualization, Y.K.; supervision, M.B.; project administration, M.B. and M.M.-e. All authors have read and agreed to the published version of the manuscript.

Funding: This research received no external funding.

Institutional Review Board Statement: Not applicable.

Informed Consent Statement: Not applicable.

Data Availability Statement: The source code, the derived terrain windows, and the raw results supporting the findings of this study are provided as Supplementary Material S1. The real terrains were extracted from the Copernicus GLO-30 DEM [49], tile N32 W007 (file Copernicus_DSM_COG_10_N32_00_W007_00_DEM), distributed by the AWS Open Data Registry; produced using Copernicus WorldDEM-30 © DLR e.V. 2010–2014 and © Airbus Defence and Space GmbH 2014–2018 provided under COPERNICUS by the European Union and ESA; all rights reserved.

Acknowledgments: During the preparation of this manuscript, the authors used Claude Opus 5.5 (Anthropic; model identifier claude-opus-5-5) for language and grammar correction. The authors have reviewed and edited the output and take full responsibility for the content of this publication.

Conflicts of Interest: The authors declare no conflicts of interest.

Abbreviations

The following abbreviations are used in this manuscript:

BTRD	Backtracking for radar deployment (the proposed exhaustive search)
BTRD+	BTRD with symmetry breaking, forward checking, and bounding
COP	Constraint optimization problem
CSP	Constraint satisfaction problem
DEM	Digital elevation model
DM	Variant with the minimum distance constraint only
FM	Full-mesh model (pairwise distance and LOS constraints)
GA	Genetic algorithm

GIS	Geographic information system
ILP	Integer linear programming
LOS	Line of sight
MCLP	Maximal covering location problem
MH	Multi-hop variant
NSGA-III	Nondominated sorting genetic algorithm III
PSO	Particle swarm optimization
UC	Unconstrained variant
WSN	Wireless sensor network

References

1. Chakrabarty, K.; Iyengar, S.S.; Qi, H.; Cho, E. Grid coverage for surveillance and target location in distributed sensor networks. *IEEE Trans. Comput.* **2002**, *51*, 1448–1453. https://doi.org/10.1109/TC.2002.1146711.
2. Akyildiz, I.F.; Su, W.; Sankarasubramaniam, Y.; Cayirci, E. Wireless sensor networks: A survey. *Comput. Netw.* **2002**, *38*, 393–422. https://doi.org/10.1016/S1389-1286(01)00302-4.
3. Huang, C.F.; Tseng, Y.C. The coverage problem in a wireless sensor network. In Proceedings of the 2nd ACM International Workshop on Wireless Sensor Networks and Applications (WSNA '03), San Diego, CA, USA, 19 September 2003; pp. 115–121. https://doi.org/10.1145/941350.941367.
4. Wang, G.; Cao, G.; La Porta, T.F. Movement-assisted sensor deployment. *IEEE Trans. Mob. Comput.* **2006**, *5*, 640–652. https://doi.org/10.1109/TMC.2006.80.
5. Xing, G.; Wang, X.; Zhang, Y.; Lu, C.; Pless, R.; Gill, C. Integrated coverage and connectivity configuration for energy conservation in sensor networks. *ACM Trans. Sens. Netw.* **2005**, *1*, 36–72. https://doi.org/10.1145/1077391.1077394.
6. Zhao, M.C.; Lei, J.; Wu, M.Y.; Liu, Y.; Shu, W. Surface coverage in wireless sensor networks. In Proceedings of the IEEE International Conference on Computer Communications (IEEE INFOCOM 2009), Rio de Janeiro, Brazil, 19–25 April 2009; pp. 109–117. https://doi.org/10.1109/INFCOM.2009.5061912.
7. Zhou, Z.; Das, S.; Gupta, H. Connected *k*-coverage problem in sensor networks. In Proceedings of the 13th International Conference on Computer Communications and Networks (ICCCN 2004), Chicago, IL, USA, 11–13 October 2004; pp. 373–378. https://doi.org/10.1109/ICCCN.2004.1401672.
8. Nakka, K.; Ammari, H.M. Hierarchical deployment and square tessellation for connected *k*-coverage in heterogeneous planar wireless sensor networks. *Acm Trans. Sens. Netw.* **2025**, *21*, 1–27. https://doi.org/10.1145/3713074.
9. Franklin, W.R. Siting observers on terrain. In *Advances in Spatial Data Handling*; Springer: Berlin/Heidelberg, Germany, 2002; pp. 109–120. https://doi.org/10.1007/978-3-642-56094-1_9.
10. Kim, Y.H.; Rana, S.; Wise, S. Exploring multiple viewshed analysis using terrain features and optimisation techniques. *Comput. Geosci.* **2004**, *30*, 1019–1032. https://doi.org/10.1016/j.cageo.2004.07.008.
11. Wang, Z.; Wang, M.; Wu, X.; Yang, S. Multi-node small radar network deployment optimization in 3D terrain. *Sensors* **2025**, *25*, 1964. https://doi.org/10.3390/s25071964.
12. Lei, Z.; Chen, X.; Tan, Y. A coverage model of FMCW radar for optimizing sensor network deployment. *IEEE/ASME Trans. Mechatronics* **2024**, *29*, 2991–3000. https://doi.org/10.1109/TMECH.2024.3396724.
13. Kar, K.; Banerjee, S. Node placement for connected coverage in sensor networks. In Proceedings of the WiOpt'03: Modeling and Optimization in Mobile, Ad Hoc and Wireless Networks, Sophia Antipolis, France, 3–5 March 2003.
14. Arora, A.; Dutta, P.; Bapat, S.; Kulathumani, V.; Zhang, H.; Naik, V.; Mittal, V.; Cao, H.; Demirbas, M.; Gouda, M.; et al. A line in the sand: A wireless sensor network for target detection, classification, and tracking. *Comput. Netw.* **2004**, *46*, 605–634. https://doi.org/10.1016/j.comnet.2004.06.007.
15. Cardei, M.; Thai, M.T.; Li, Y.; Wu, W. Energy-efficient target coverage in wireless sensor networks. In Proceedings of the IEEE Conference on Computer Communications (IEEE INFOCOM 2005), Miami, FL, USA, 13–17 March 2005; Volume 3, pp. 1976–1984. https://doi.org/10.1109/INFCOM.2005.1498475.
16. Cardei, M.; Du, D.Z. Improving wireless sensor network lifetime through power aware organization. *Wirel. Netw.* **2005**, *11*, 333–340. https://doi.org/10.1007/s11276-005-6615-6.
17. Cardei, M.; Wu, J.; Lu, M.; Pervaiz, M.O. Maximum network lifetime in wireless sensor networks with adjustable sensing ranges. In Proceedings of the IEEE International Conference on Wireless and Mobile Computing, Networking and Communications (WiMob 2005), Montreal, QC, Canada, 22–24 August 2005; Volume 3, pp. 438–445. https://doi.org/10.1109/WIMOB.2005.1512935.
18. Zhang, H.; Wang, H.; Feng, H. A distributed optimum algorithm for target coverage in wireless sensor networks. In Proceedings of the 2009 Asia-Pacific Conference on Information Processing (APCIP), Shenzhen, China, 18–19 July 2009; pp. 144–147. https://doi.org/10.1109/APCIP.2009.172.

19. Yu, Y.; Prasanna, V.K. Energy-balanced task allocation for collaborative processing in wireless sensor networks. *Mob. Netw. Appl.* **2005**, *10*, 115–131. https://doi.org/10.1023/B:MONE.0000048550.31717.c5.
20. Meguerdichian, S.; Koushanfar, F.; Potkonjak, M.; Srivastava, M.B. Coverage problems in wireless ad-hoc sensor networks. In Proceedings of the IEEE Conference on Computer Communications (IEEE INFOCOM 2001), Anchorage, AK, USA, 22–26 April 2001; Volume 3, pp. 1380–1387. https://doi.org/10.1109/INFCOM.2001.916633.
21. Chen, A.; Kumar, S.; Lai, T.H. Designing localized algorithms for barrier coverage. In Proceedings of the 13th Annual ACM International Conference on Mobile Computing and Networking (MobiCom '07), Montréal, QC, Canada, 9–14 September 2007; pp. 63–74. https://doi.org/10.1145/1287853.1287862.
22. Cardei, M.; Wu, J. Energy-efficient coverage problems in wireless ad-hoc sensor networks. *Comput. Commun.* **2006**, *29*, 413–420. https://doi.org/10.1016/j.comcom.2004.12.025.
23. Howard, A.; Matarić, M.J.; Sukhatme, G.S. An incremental self-deployment algorithm for mobile sensor networks. *Auton. Robot.* **2002**, *13*, 113–126. https://doi.org/10.1023/A:1019625207705.
24. Poduri, S.; Sukhatme, G.S. Constrained coverage for mobile sensor networks. In Proceedings of the IEEE International Conference on Robotics and Automation (ICRA 2004), New Orleans, LA, USA, 26 April–1 May 2004; Volume 1, pp. 165–171. https://doi.org/10.1109/ROBOT.2004.1307146.
25. Osmani, A.; Dehghan, M.; Pourakbar, H.; Emdadi, P. Fuzzy-based movement-assisted sensor deployment method in wireless sensor networks. In Proceedings of the First International Conference on Computational Intelligence, Communication Systems and Networks (CICSyN 2009), Indore, India, 23–25 July 2009; pp. 90–95. https://doi.org/10.1109/CICSYN.2009.97.
26. Bai, X.; Yun, Z.; Xuan, D.; Lai, T.H.; Jia, W. Optimal patterns for four-connectivity and full coverage in wireless sensor networks. *IEEE Trans. Mob. Comput.* **2010**, *9*, 435–448. https://doi.org/10.1109/TMC.2009.143.
27. Li, X.Y.; Wan, P.J.; Frieder, O. Coverage in wireless ad-hoc sensor networks. In Proceedings of the IEEE International Conference on Communications (ICC 2002), New York, NY, USA, 28 April–2 May 2002; Volume 5, pp. 3174–3178. https://doi.org/10.1109/ICC.2002.997421.
28. Carbunar, B.; Grama, A.; Vitek, J.; Carbunar, O. Redundancy and coverage detection in sensor networks. *ACM Trans. Sens. Netw.* **2006**, *2*, 94–128. https://doi.org/10.1145/1138127.1138131.
29. Chatzigiannakis, I.; Mylonas, G.; Nikoletseas, S. Modeling and evaluation of the effect of obstacles on the performance of wireless sensor networks. In Proceedings of the 39th Annual Simulation Symposium (ANSS'06), San Diego, CA, USA, 2–6 April 2006; pp. 50–60. https://doi.org/10.1109/ANSS.2006.26.
30. Wang, Y.C.; Hu, C.C.; Tseng, Y.C. Efficient deployment algorithms for ensuring coverage and connectivity of wireless sensor networks. In Proceedings of the First International Conference on Wireless Internet (WICON'05), Budapest, Hungary, 10–15 July 2005; pp. 114–121. https://doi.org/10.1109/WICON.2005.13.
31. Zou, Y.; Chakrabarty, K. Sensor deployment and target localization in distributed sensor networks. *ACM Trans. Embed. Comput. Syst.* **2004**, *3*, 61–91. https://doi.org/10.1145/972627.972631.
32. Rouault, E.; Warmerdam, F.; Schwehr, K.; Kiselev, A.; Butler, H.; Łoskot, M.; Szekeres, T.; Tourigny, E.; Landa, M.; Miara, I.; et al. GDAL. In *Zenodo*, v3.13.3; OSGeo: Beaverton, OR, USA, 2026. https://doi.org/10.5281/zenodo.5884351.
33. Wang, J.; Robinson, G.J.; White, K. Generating viewsheds without using sightlines. *Photogramm. Eng. Remote Sens.* **2000**, *66*, 87–90.
34. Wang, Y.; Dou, W. Accurate calculation method of terrain viewshed for wireless signal as line of sight. *Trans. GIS* **2024**, *28*, 1236–1253. https://doi.org/10.1111/tgis.13188.
35. Zhou, X.; Wang, W.; Huang, Q.; Feng, N.; Han, P.; Wu, C. Sparse multi-viewshed analysis for assisting video surveillance network location optimization. In Proceedings of the 36th Chinese Control and Decision Conference (CCDC), Xi'an, China, 25–27 May 2024; pp. 1687–1694. https://doi.org/10.1109/CCDC62350.2024.10587971.
36. Leenders, N.; van Oijen, J.; Lindelauf, R.; Cule, B. Uncertainty in visibility: A scoping review of the probable and fuzzy viewshed for observer location optimization. *Int. J. Geogr. Inf. Sci.* **2026**, *40*, 1993–2022. https://doi.org/10.1080/13658816.2025.2581833.
37. Abrams, Z.; Goel, A.; Plotkin, S. Set *k*-cover algorithms for energy efficient monitoring in wireless sensor networks. In Proceedings of the 3rd International Symposium on Information Processing in Sensor Networks (IPSN '04), Berkeley, CA, USA, 26–27 April 2004; pp. 424–432. https://doi.org/10.1145/984622.984684.
38. Hefeeda, M.; Bagheri, M. Randomized *k*-coverage algorithms for dense sensor networks. In Proceedings of the IEEE International Conference on Computer Communications (IEEE INFOCOM 2007), Anchorage, AK, USA, 6–12 May 2007; pp. 2376–2380. https://doi.org/10.1109/INFCOM.2007.284.
39. Church, R.; ReVelle, C. The maximal covering location problem. *Pap. Reg. Sci. Assoc.* **1974**, *32*, 101–118. https://doi.org/10.1007/BF01942293.
40. Quintão, F.P.; Nakamura, F.G.; Mateus, G.R. Evolutionary algorithm for the dynamic coverage problem applied to wireless sensor networks design. In Proceedings of the 2005 IEEE Congress on Evolutionary Computation (CEC 2005), Edinburgh, UK, 2–5 September 2005; Volume 2, pp. 1589–1596. https://doi.org/10.1109/CEC.2005.1554879.

41. Megerian, S.; Koushanfar, F.; Potkonjak, M.; Srivastava, M.B. Worst and best-case coverage in sensor networks. *IEEE Trans. Mob. Comput.* **2005**, *4*, 84–92. https://doi.org/10.1109/TMC.2005.15.
42. Habib, S.J.; Safar, M. Sensitivity study of sensors' coverage within wireless sensor networks. In Proceedings of the 16th International Conference on Computer Communications and Networks (ICCCN 2007), Honolulu, HI, USA, 13–16 August 2007; pp. 876–881. https://doi.org/10.1109/ICCCN.2007.4317928.
43. Dhillon, S.S.; Chakrabarty, K. Sensor placement for effective coverage and surveillance in distributed sensor networks. In Proceedings of the IEEE Wireless Communications and Networking Conference (WCNC 2003), New Orleans, LA, USA, 16–20 March 2003; Volume 3, pp. 1609–1614. https://doi.org/10.1109/WCNC.2003.1200627.
44. Abul, O.; Savsatli, F. Geospatial radar deployment optimization. In Proceedings of the 6th International Conference on Computer Science and Engineering (UBMK), Ankara, Turkey, 15–17 September 2021; pp. 440–445. https://doi.org/10.1109/UBMK52708.2021.9558967.
45. Li, H.P.; Feng, D.Z.; Chen, S.F.; Zhou, Y.P. Deployment optimization method of multistatic radar for constructing circular barrier coverage. *Sensors* **2021**, *21*, 6573. https://doi.org/10.3390/s21196573.
46. Priyadarshi, R. Efficient node deployment for enhancing coverage and connectivity in wireless sensor networks. *Sci. Rep.* **2025**, *15*, 29052. https://doi.org/10.1038/s41598-025-14252-0.
47. Moslehi, M.M. Exploring coverage and security challenges in wireless sensor networks: A survey. *Comput. Netw.* **2025**, *260*, 111096. https://doi.org/10.1016/j.comnet.2025.111096.
48. Löffler, S.; Kroll, F.; Becker, I.; Hofstedt, P. Optimal beacon placement for indoor positioning using constraint programming. In Proceedings of the 19th IEEE/ACS International Conference on Computer Systems and Applications (AICCSA), Abu Dhabi, United Arab Emirates, 5–7 December 2022; pp. 1–8. https://doi.org/10.1109/AICCSA56895.2022.10017575.
49. European Space Agency. *Copernicus DEM—Global and European Digital Elevation Model*; Dataset; CDSE: Linthicum Heights, MD, USA, 2022. https://doi.org/10.5270/ESA-c5d3d65.
50. Perron, L.; Didier, F. *CP-SAT*, version 9.15, Google OR-Tools; Google LLC: Mountain View, CA, USA, 2026. Available online: https://developers.google.com/optimization/cp/cp_solver/ (accessed on 20 September 2026).
51. Benelallam, I. Approches Complètes pour la réSolution des Problèmes DisCSPs et DCOPs. Ph.D. Thesis, Université Mohammed V-Agdal, Rabat, Morocco, 2010.
52. Dechter, R.; van Beek, P. Local and global relational consistency. *Theor. Comput. Sci.* **1997**, *173*, 283–308. https://doi.org/10.1016/S0304-3975(97)86737-0.
53. Rossi, F.; Petrie, C.; Dhar, V. On the equivalence of constraint satisfaction problems. In Proceedings of the 9th European Conference on Artificial Intelligence (ECAI 90), Stockholm, Sweden, 6–10 August 1990; pp. 550–556.
54. Ehrgott, M. *Multicriteria Optimization*, 2nd ed.; Springer: Berlin/Heidelberg, Germany, 2005. https://doi.org/10.1007/3-540-27659-9.
55. Skolnik, M.I. *Introduction to Radar Systems*, 3rd ed.; McGraw-Hill: New York, NY, USA, 2001.
56. Doerry, A.W. *Earth Curvature and Atmospheric Refraction Effects on Radar Signal Propagation*; Technical Report SAND2012-10690; Sandia National Laboratories: Albuquerque, NM, USA, 2013. https://doi.org/10.2172/1088060.
57. Gent, I.P.; Petrie, K.E.; Puget, J.F. Symmetry in constraint programming. In *Handbook of Constraint Programming*; Rossi, F., van Beek, P., Walsh, T., Eds.; Elsevier: Amsterdam, The Netherlands, 2006; pp. 329–376. https://doi.org/10.1016/S1574-6526(06)80014-3.
58. Haralick, R.M.; Elliott, G.L. Increasing tree search efficiency for constraint satisfaction problems. *Artif. Intell.* **1980**, *14*, 263–313. https://doi.org/10.1016/0004-3702(80)90051-X.
59. Nethercote, N.; Stuckey, P.J.; Becket, R.; Brand, S.; Duck, G.J.; Tack, G. MiniZinc: Towards a standard CP modelling language. In Proceedings of the Principles and Practice of Constraint Programming—CP 2007, Berlin/Heidelberg, Germany, 23–27 September 2007; Lecture Notes in Computer Science; Volume 4741, pp. 529–543. https://doi.org/10.1007/978-3-540-74970-7_38.
60. Perron, L.; Didier, F.; Gay, S. The CP-SAT-LP Solver (Invited Talk). In Proceedings of the 29th International Conference on Principles and Practice of Constraint Programming (CP 2023), Toronto, ON, Canada, 27–31 August 2023; Leibniz International Proceedings in Informatics (LIPIcs); Volume 280, pp. 3:1–3:2. https://doi.org/10.4230/LIPIcs.CP.2023.3.
61. Nemhauser, G.L.; Wolsey, L.A.; Fisher, M.L. An analysis of approximations for maximizing submodular set functions—I. *Math. Program.* **1978**, *14*, 265–294. https://doi.org/10.1007/BF01588971.

Disclaimer/Publisher's Note: The statements, opinions and data contained in all publications are solely those of the individual author(s) and contributor(s) and not of MDPI and/or the editor(s). MDPI and/or the editor(s) disclaim responsibility for any injury to people or property resulting from any ideas, methods, instructions or products referred to in the content.